Track Impact Parameter Resolution Analysis of the BaBar Detector

Marc L'Heureux
U. of British Columbia
Jul 23, 2002

1 Introduction

The BaBar Detector is designed to study the different states and decays of the B meson. This involves creation of the B mesons from colliding an electron beam with a positron beam. When the beams collide many different things may happen, called events. Events may be the decay of a B meson or other interactions between the positrons and electrons. To understand what happens in any one event requires the ability to observe the sub-atomic particles resulting from an event.

To detect the sub-atomic particles that result from the colliding beams, several different parts of the detector are used. Large electro-magnets create a magnetic field so that charged particle tracks will curve rather than move in a straight line. For this reason, reconstructed track paths are called track helices. The first components that detect the particles are the silicon vertex detectors. These are plates of silicon that surround the beam pipe and record charged hits where the particle passes through a plate. Another component that records charged hits is the drift chamber. The drift chamber surrounds the silicon vertex detectors and is a sealed chamber which contains a gas. The chamber contains numerous wires that will record a hit when a charged particle comes near. The position of the hit is determined from which wire detected the hit and how far from the wire it was (based on signal time).

Certain measurements of the B meson decay require a good understanding of the resolution of the detector in the z direction. If any meson has an appreciable lifetime, it will travel a certain distance along the z direction before decaying. In events where a B meson and a $\bar{B}$ meson are created from an $\Upsilon(4S)$ particle, finding the separation between the spots where these mesons decay allows us to study CP asymmetries. This is really the comparison between B mesons and a CP state or $\bar{B}$ mesons and a CP state, as well as whether there was a meson decay first or a CP state first. Comparisons between these reveal the CP asymmetry. Often the distance separating spots of meson decays are very small (the differences in lifetimes are small), so observations of this separation are difficult. Much of the time these measurements are with error, introducing errors into the measurements of the CP asymmetry.

Another measurement where resolution is of importance is for the observation of $B \to \bar{B}$. As a B meson travels along the z direction, mixing causes it to undergo the change from a B meson to a $\bar{B}$ meson. The resolution of the detector in the z direction has a direct bearing on the amplitude in which the change of $B \to \bar{B}$ can be measured. If a B meson can decay to a μ^+ and a $\bar{B}$ meson can decay to a μ^-, then

$$\frac{\mu^+\mu^- - (\mu^+\mu^+ + \mu^-\mu^-)}{\text{all } \mu\mu} \tag{1}$$

will reveal a percentage of the meson's mixing. When this expression is compared against Δz, a steady fluctuation is revealed from one B meson state to the next. However, with a poor resolution in z, this fluctuation may be diminished in amplitude. An understanding of the resolution of the detector can help correct for such measurements.

2 Track Helix Parameters

Hits from the silicon vertex detector and the drift chamber are collected and used in a computer algorithm that creates a track helix that has several parameters: ϕ_0, $\tan\lambda$, d_0, z_0 and ω. First, ϕ_0 is the angle of the particle with respect to the x-y plane. This ranges from π to $-\pi$. The $\tan\lambda$ parameter describes the track's angle from the z axis. The next parameter, d_0 is the distance of closest approach to the origin for the helix. This value is signed according to track direction. The z_0 parameter is simply the z co-ordinate of the point where the track begins. Lastly, ω is the curvature of the track helix due to the electro-magnets.

Errors of these parameters are calculated from the fit of the helix. Tracks with fewer hits have a greater uncertainty associated with them. The ability of the detector to record sufficient hits and reconstruct the track helix from these hits determines the detector's resolution.

If the resolution of the detector was perfect then the difference between z_0 of two tracks that originated from the same spot would be exactly zero. As well, the sum of the d_0 would result in zero. However, since track helices are pieced together from a number of hits from mainly the silicon vertex detectors and the drift chamber, the track is not always traced back to its point of origin accurately. Some particles experience Rutherford scattering as they pass through the walls of the beam pipe or other supports of the detector, therefore, later hits may not align properly with earlier hits for such particles.

3 Event Selection

The first stage of collecting data was determining the nature of the best events to use in this analysis. As noted above, events where the tracks originate from the same point are of the most use in this analysis. Events which involve mesons with relatively long lifetimes are undesirable. Such mesons may move some distance in the beam pipe before decaying, often involving several subatomic particles. This is an unnecessary complexity. Other more desirable events immediately result in the creation of two oppositely charged particles which originate from the same spot and move directly away from each other (because of conservation of momentum).

In order to obtain these events, the `IsPhysicsEvents` category from the Objectivity database in the Beta package at BaBar was used. Run numbers 16449-16451, 16765-16948 were used. All data was stored into an ntuple: a collection of data that can be used to make a histogram. In the ntuple generation code two cuts were placed on the data that would be placed into the ntuple. The first cut allowed any event which had three or less tracks from the good tracks loose category. The second cut accepted the event only if there were tracks of opposite charge inside the event. For each track that passed these cuts certain values were stored inside the ntuple. These were the number of tracks, momentum and center-of-mass momentum (the magnitude of each as well as in the $\hat{x}$, $\hat{y}$ and $\hat{z}$ directions), the beamspot x, y, and z values, the charge of the track, and the helix parameters: z_0, d_0, ϕ_0, $\tan(\lambda)$, and ω, as well as their associated errors and rotated values.

ROOT was used to make histograms from the ntuples created by the Beta code. A ROOT class was used to build these histograms. Inside this class further cuts were imposed. The first was that all events were required to have only two tracks. Only two tracks are necessary in order to obtain the proper physics events that originate from one point. Because these events create two oppositely charged tracks, each of the two tracks were required to be of opposite charge. Cuts were placed on the transverse momentum of tracks so that the absolute value of the center-of-mass momentum in the $\hat{x}$ direction of both tracks added together was less than .1 GeV/c. As well, the absolute value of the center-of-mass momentum in the $\hat{y}$ direction of both tracks added together was less than .1 GeV/c. Cosmic rays were eliminated by removing pairs of tracks where the absolute value of the sum of both track's $\hat{z}$ momentum in the lab frame was less than 0.1 GeV/c. The track building software normally makes two tracks from the single cosmic ray particle, but since the momentum in the $\hat{z}$ direction for both tracks is just the momentum in the $\hat{z}$ direction for the cosmic ray, this cut will eliminate these tracks. The final cut was placed on tracks which had a high z_0 error. These tracks were obtained from an insufficient number of hits on the silicon vertex detector due to the shape of the detector (there are less detectors at the rear), so it is possible that an unrelated hit may be included to create the track helix parameters. Any event which had an associated z_0 error of greater than 0.1 cm for either track was cut.

The remaining events were of Bhabha, Two-Photon or μ-pair type. The tracks of these events originate from the same point, create particles of opposite charge, and are exactly opposite in transverse directions. Because of this, the resolution can be accurately studied with respect to the $\hat{z}$ direction. This is accomplished by studying the difference in z_0 between each of the two tracks. Studying the sum of d_0's for tracks allows the resolution in the x and y directions to be studied.

4 Track Corrections

Before the track data can be used, several corrections must be made to correct for an non-centered beam which direction does not lie directly along the z axis. The beam direction, $\vec{B}$ was found by:

$$
\begin{aligned}
B_x &= \sin(\theta)\cos(\phi_0) && (2)\\
B_y &= \sin(\theta)\sin(\phi_0) && (3)\\
B_z &= \cos(\theta) && (4)
\end{aligned}
$$

The values for θ and ϕ_0 are obtained from the `HepLorentzVector CMFrame` class from the BaBar framework. The beam spot vector $\vec{b}_0$ was taken directly from the x, y and z values from the `HepPoint Beamspot` class in the BaBar framework. The dimensions of the beam are roughly 150 μm in x and 50 μm in y, but more than 1 cm in z.

To correct the z_0 and d_0 values, the track vector is translated along its direction vector until the point that is closest to the beam is reached. The track vector, $\vec{u}$, the track velocity vector, $\vec{v}$, and the track curvature vector, $\vec{\omega}$ are given by:

$$
\begin{aligned}
\vec{u}_0 &= (\ -d_0\sin\phi_0,\ d_0\cos\phi_0,\ z_0\ ) && (5)\\
\vec{v}_0 &= (\ \cos\phi_0,\ \sin\phi_0,\ \tan\lambda\ ) && (6)\\
\vec{\omega}_0 &= (\ -\omega\sin\phi_0,\ \omega\cos\phi_0,\ 0\ ) && (7)
\end{aligned}
$$

where d_0, ϕ_0 and z_0 are the original d_0, ϕ_0 and z_0 of the BaBar coordinate system. A distance s is calculated, using the two dimensional dot product:

$$
s_0 = (\vec{b}_0 - \vec{u}_0)_{x,y} \cdot \vec{v}_{0_{x,y}} \tag{8}
$$

The values of $\vec{u}_0$ and $\vec{v}_0$ can then be translated along the beam direction to find a z_0 that is closer to the beamspot than that originally obtained from the raw data.

$$
\begin{aligned}
\vec{u}_1 &= \vec{u}_0 + s_0\vec{v}_0 + \frac{s_0^2}{2}\vec{\omega}_0 && (9)\\
\vec{v}_1 &= \vec{v}_0 + s_0\vec{\omega}_0 && (10)
\end{aligned}
$$

The average of z_0 for these translated tracks is used to find a new z co-ordinate for the beam spot. This z_{avg} is then used to eliminate some of the smearing of the beam coordinate so that a more precise beam coordinate can be used.

$$
\vec{b}_1 = \vec{b}_0 + (z_{avg} - b_z)B_z \tag{11}
$$

With a more accurate beamspot the distance s may be calculated again, so equations 8 through 10 are repeated.

$$
s_1 = (\vec{b}_1 - \vec{u}_0)_{x,y} \cdot \vec{v}_{0_{x,y}} \tag{12}
$$

$$\begin{aligned}
\vec{u}_2 &= \vec{u}_0 + s_1\vec{v}_0 + \frac{s_1^2}{2}\vec{\omega}_0 && (13)\\
\vec{v}_2 &= \vec{v}_0 + s_1\vec{\omega}_0 && (14)
\end{aligned}$$

After this, the coordinate system is centered on the beamspot.

$$\begin{aligned}
\vec{u}_3 &= \vec{u}_2 - \vec{b}_1 && (15)\\
\vec{v}_3 &= \vec{v}_2 && (16)
\end{aligned}$$

A rotation matrix is created so that the position and velocity vectors may be rotated to a coordinate system which has the beam direction directly along the z axis. This matrix is created using the $\vec{B}$ vector found from `CMFrame`.

$$M_R = \begin{bmatrix} \frac{B_z}{\sqrt{1-b_y^2}} & 0 & -\frac{B_x}{\sqrt{1-b_y^2}} \\ -\frac{B_x B_y}{\sqrt{1-b_y^2}} & \sqrt{1-b_y^2} & -\frac{B_y B_z}{\sqrt{1-b_y^2}} \\ B_x & B_y & B_z \end{bmatrix} \tag{17}$$

The position and velocity vectors are rotated as follows:

$$\begin{aligned}
\vec{u}_R &= [M_R][\vec{u}_3] && (18)\\
\vec{v}_R &= [M_R][\vec{v}_3] && (19)
\end{aligned}$$

Finally, the resulting rotated d_0, d_{0_R}, may be found, using the equation

$$d_{0_R} = -\frac{u_{R_x} v_{R_y} - u_{R_y} v_{R_x}}{\sqrt{v_{R_x}^2 + v_{R_y}^2}} \tag{20}$$

and the rotated z_0, z_{0_R}, is simply the z coordinate of the u_R vector:

$$z_{0_R} = u_{R_z} \tag{21}$$

After this, the difference of z_{R_0} and the sum of d_{R_0} between the tracks were directly calculated. The difference of z_{R_0} was divided by further errors than just that from the track fitting parameters. These further errors were a correction for the beam size. The mathematical expression used for the difference of z_{R_0} divided by errors is:

$$\frac{z_{R_0} - z_{R_1}}{\sqrt{\sigma_{z_{corr_0}}^2 + \sigma_{z_{corr_1}}^2}} \tag{22}$$

where

$$\sigma_{z_{corr_0}} = z^2_{err_0} + (\sigma_x \cos\phi_0 \tan\lambda_0)^2 + (\sigma_y \sin\phi_0 \tan\lambda_0)^2 \tag{23}$$

$$\sigma_{z_{corr_1}} = z^2_{err_1} + (\sigma_x \cos\phi_1 \tan\lambda_1)^2 + (\sigma_y \sin\phi_1 \tan\lambda_1)^2 \tag{24}$$

and $\sigma_x = 0.015$ cm and $\sigma_y = 0.005$ cm. The subscripts indicate the track number, err is the error on that value and R indicates a rotated value. For the sum of d_{R_0} the mathematical expression is:

$$\frac{d_{R_0} + d_{R_1}}{\sqrt{d^2_{err_0} + d^2_{err_1}}} \tag{25}$$

where the subscripts again indicate track number and R a rotated value. High statistics were used to observe the deviation from zero for these calculations. When this was done, the d_0 sum histogram had a mean of roughly -0.2. For this reason both the positive and negative values of equation 25 were added to a histogram, so that the histogram has a mean of exactly zero.

5 Fits

A number of different functions were tried to fit the histograms of the z_0 difference divided by errors and the d_0 sum divided by errors. As well as these histograms, slices in the y direction of both histograms as functions of other quantities were fit. These other quantities these two histograms were plotted against were momentum, center-of-mass momentum, ϕ_0, θ, and a scattering function. This scattering function is motivated by Rutherford scattering. For the D0 sum histogram, this scattering function is:

$$\sqrt{\frac{1}{P_0^2 \sin^3\theta_0} + \frac{1}{P_1^2 \sin^3\theta_1}} \tag{26}$$

where P_0 and P_1 is momentum and the subscripts refer to the track number. The subscripts are likewise defined for θ_0 and θ_1. For the z_0 difference histogram, the scattering function is:

$$\sqrt{\frac{1}{P_0^2 \sin^5\theta_0} + \frac{1}{P_1^2 \sin^5\theta_1}} \tag{27}$$

The first fit tried for these histograms was a central Gaussian which had tails described by a power law. This function is:

$$Ae^{-\frac{x'^2}{2}} + B \begin{bmatrix} |x'| \geq \sqrt{3} & (\frac{3}{e})^{\frac{3}{2}} |x'|^{-3} \\ |x'| < \sqrt{3} & e^{-\frac{x'^2}{2}} \end{bmatrix} \tag{28}$$

where $x' = \frac{x-C}{\sigma}$. A, B, C and σ are all parameters of the fit. The power law is derived from Rutherford scattering. When Rutherford scattering is projected into two dimensions, the scattering is described by a power law of -3. A simple function of x^{-3} is tangent to a Gaussian function at $\sqrt{3}$, so once the x^3 function is normalized it will join with the Gaussian smoothly. However, this function fit poorly in some cases. If the top of the histogram was too wide, the function tapered prematurely, lifting the tails of the function far from the actual histogram. Generally, the fits were not good at the beginning of the tails either.

The second function was similar to the first function, but the power of the tail piece was allowed to vary as a parameter. This function is:

$$A\left\{(1-B)e^{-\frac{x'^2}{2}} + B\begin{bmatrix} |x'| \geq \sqrt{3} & (\frac{|E|}{e})^{\frac{E}{2}}|x'|^{-E} \\ |x'| < \sqrt{3} & e^{-\frac{x'^2}{2}} \end{bmatrix} + K\right\} \tag{29}$$

where again $x' = \frac{x-C}{\sigma}$, B is the fraction of the function between the Gaussian part and the power law part, E is the power parameter and K is a simple constant. This fit was also used with the log likelihood option in ROOT to better account for bins with only one or no entry at the tails. The constant term, K, sometimes dominated the tails and emphasis on the power law was decreased. For this reason another function was tried.

The third function is the same as the second, but a fixed power was used again and the constant was eliminated. This function is:

$$A\left\{(1-B)e^{-\frac{x'^2}{2}} + B\begin{bmatrix} |x'| \geq \sqrt{3} & (\frac{|3|}{e})^{\frac{3}{2}}|x'|^{-3} \\ |x'| < \sqrt{3} & e^{-\frac{x'^2}{2}} \end{bmatrix}\right\} \tag{30}$$

This function had the same problems fitting as the first: if the Gaussian was wide the tails might taper prematurely and there was poor fitting at the very beginning of the tails.

The fourth function was an effort to allow the Gaussian peak to connect with the power law tail function at a place other than $\sqrt{3}$ sigma. This function is:

$$A\begin{bmatrix} |x'| \geq F & \frac{e^{\frac{E^2}{2}}(E)(F)^{E-2}}{|x'|^E-(F^E-(E)(F)^{E-2})} \\ |x'| < F & e^{-\frac{x'^2}{2}} \end{bmatrix} \tag{31}$$

where $x' = \frac{x-C}{\sigma}$. This function fit reasonably well and gave smooth changes in parameters between histogram slices.

Residuals obtained by subtracting this function from the histogram showed a pattern at the peak that suggested adding another Gaussian would improve the fit. In response, this function was tried:

$$A\left\{(1-B)\begin{bmatrix} |x'| \geq F & \frac{e^{\frac{E^2}{2}}(E)(F)^{E-2}}{|x'|^E-(F^E-(E)(F)^{E-2})} \\ |x'| < F & e^{-\frac{x_1'^2}{2}} \end{bmatrix} + Be^{-\frac{x_2'^2}{2}}\right\} \tag{32}$$

where $x_1' = \frac{x-C}{\sigma_1}$ and $x_2' = \frac{x-C}{\sigma_2}$. However, during the fit the parameter B was occasionally chosen to be negative, and sometimes σ_2 was reduced to zero.

A sixth function whose parameters would consistently have values of meaning was then used. This function is:

$$\frac{A}{2}\left(\begin{bmatrix} |x_1'| \geq F & \frac{e^{\frac{E^2}{2}}(E)(F)^{E-2}}{|x_1'|^E-(F^E-(E)(F)^{E-2})} \\ |x_1'| < F & e^{-\frac{x_1'^2}{2}} \end{bmatrix} + \begin{bmatrix} |x_2'| \geq F & \frac{e^{\frac{E^2}{2}}(E)(F)^{E-2}}{|x_2'|^E-(F^E-(E)(F)^{E-2})} \\ |x_2'| < F & e^{-\frac{x_2'^2}{2}} \end{bmatrix}\right) \tag{33}$$

where $x_1' = \frac{x-C}{|\sigma-\delta\sigma|}$ and $x_2' = \frac{x-C}{|\sigma+\delta\sigma|}$.

6 Figures

The figures included are of three types: histogram slices with fits, residuals for these fits, and graphs of fit parameters. Initially, two-dimensional histograms were created: z_0 difference divided by errors and d_0 sum divided by errors as functions of momentum, center-of-mass momentum, ϕ_0 and θ. Eleven equal slices in Y of these histograms were made, and each were fit with the function described by equation 33. These eleven slices were labeled `_Y#` (where `#` indicates the slice number. A slice in X was also made, and was labeled `_X`. The residuals are labeled in an identical manner. These were created by subtracting the fit function from the value of the histogram.

The graphs that accompany these histograms are the fit parameters as they vary with bin number, or the slice number (there are 100 bins in X for each histogram). Table 1 relates the parameter names from the figures to the variables in equation 33.

Table 1: Parameters of Equation 33

Variable	Parameter Name
A	Height
C	Mean
E	Tail-power
F	Tail-tangent
σ	Sigma
$\delta\sigma$	Delta Sigma

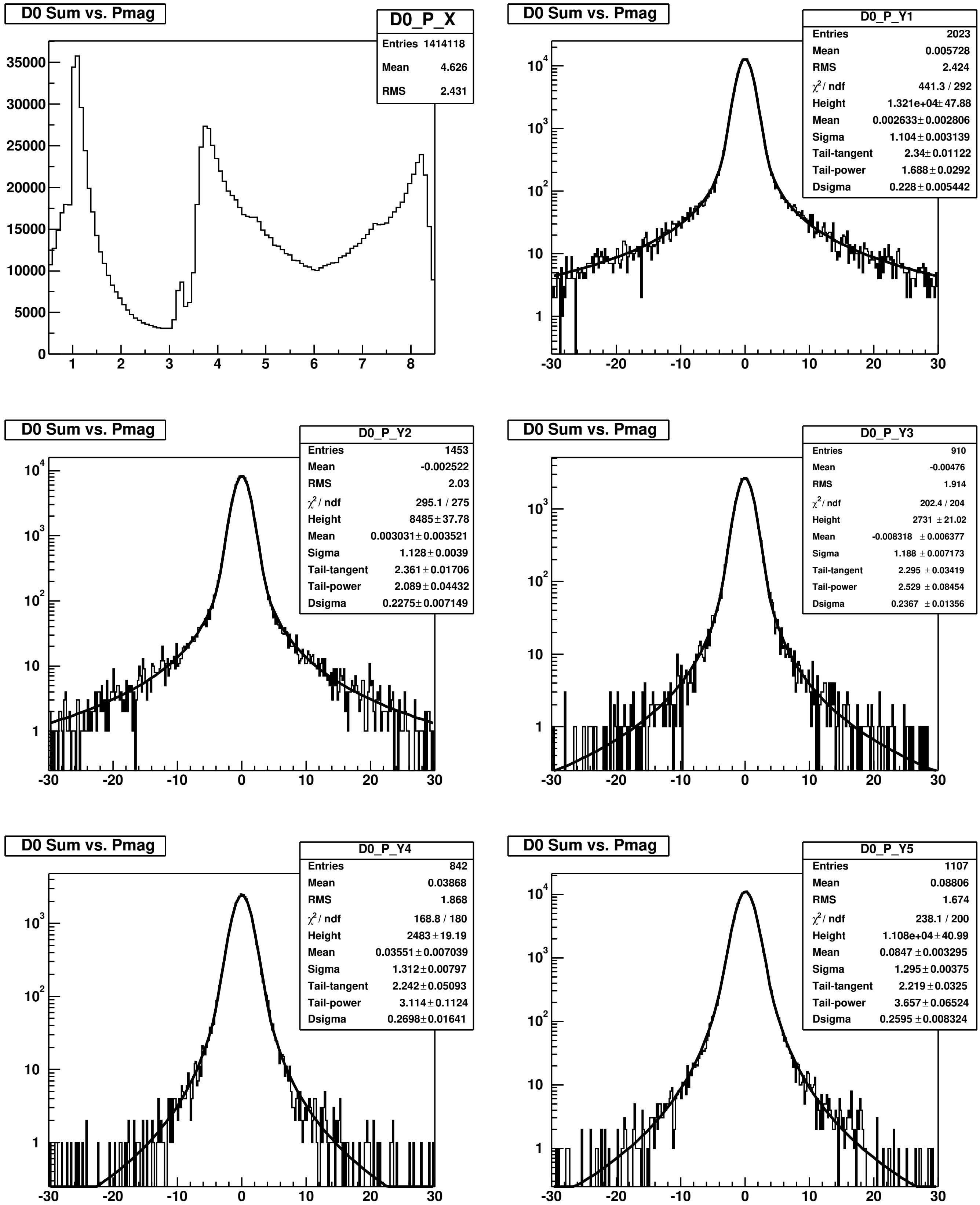

Figure 1: d_0 Sum divided by errors as a function of momentum fit with equation 33

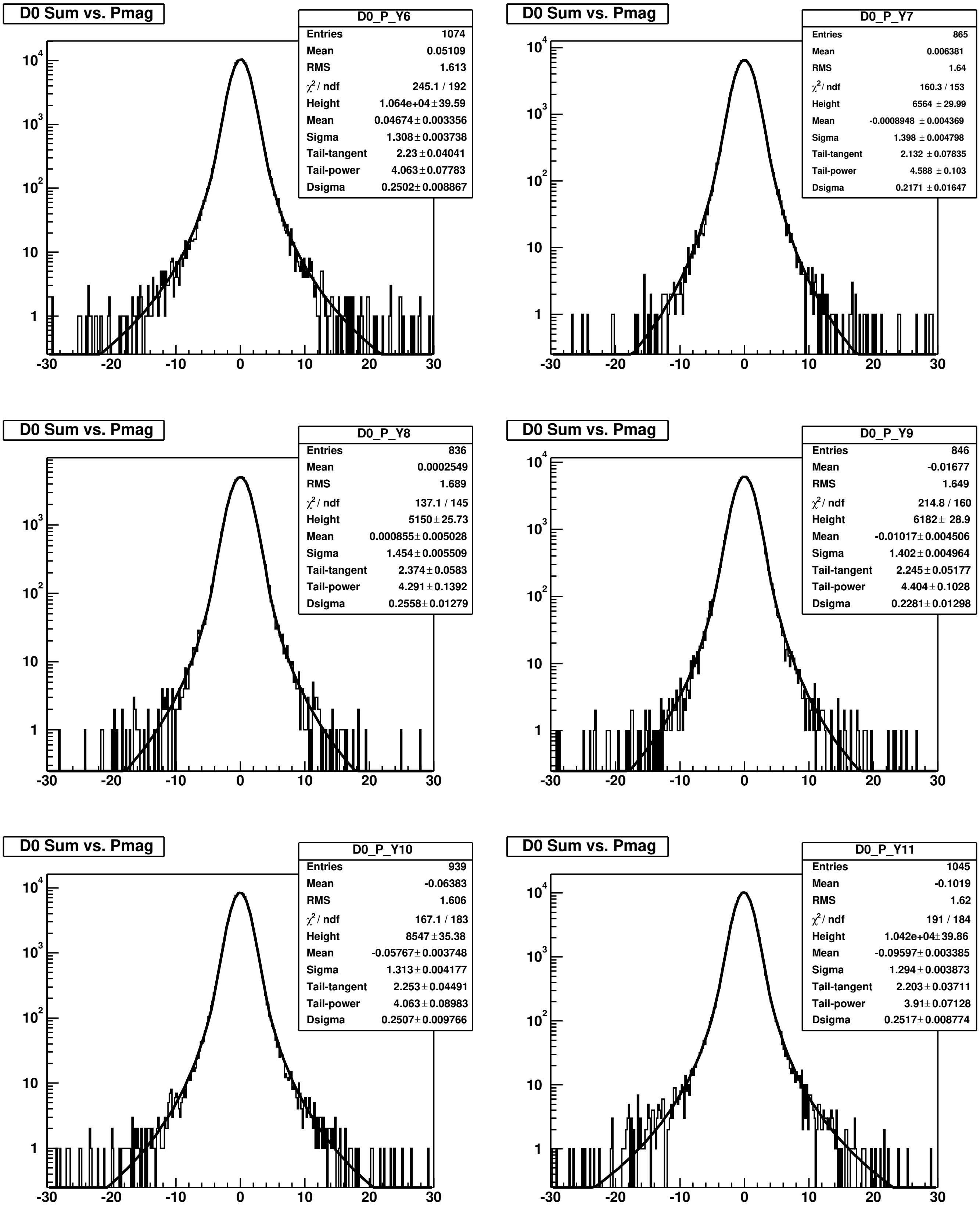

Figure 2: d_0 Sum divided by errors as a function of momentum fit with equation 33

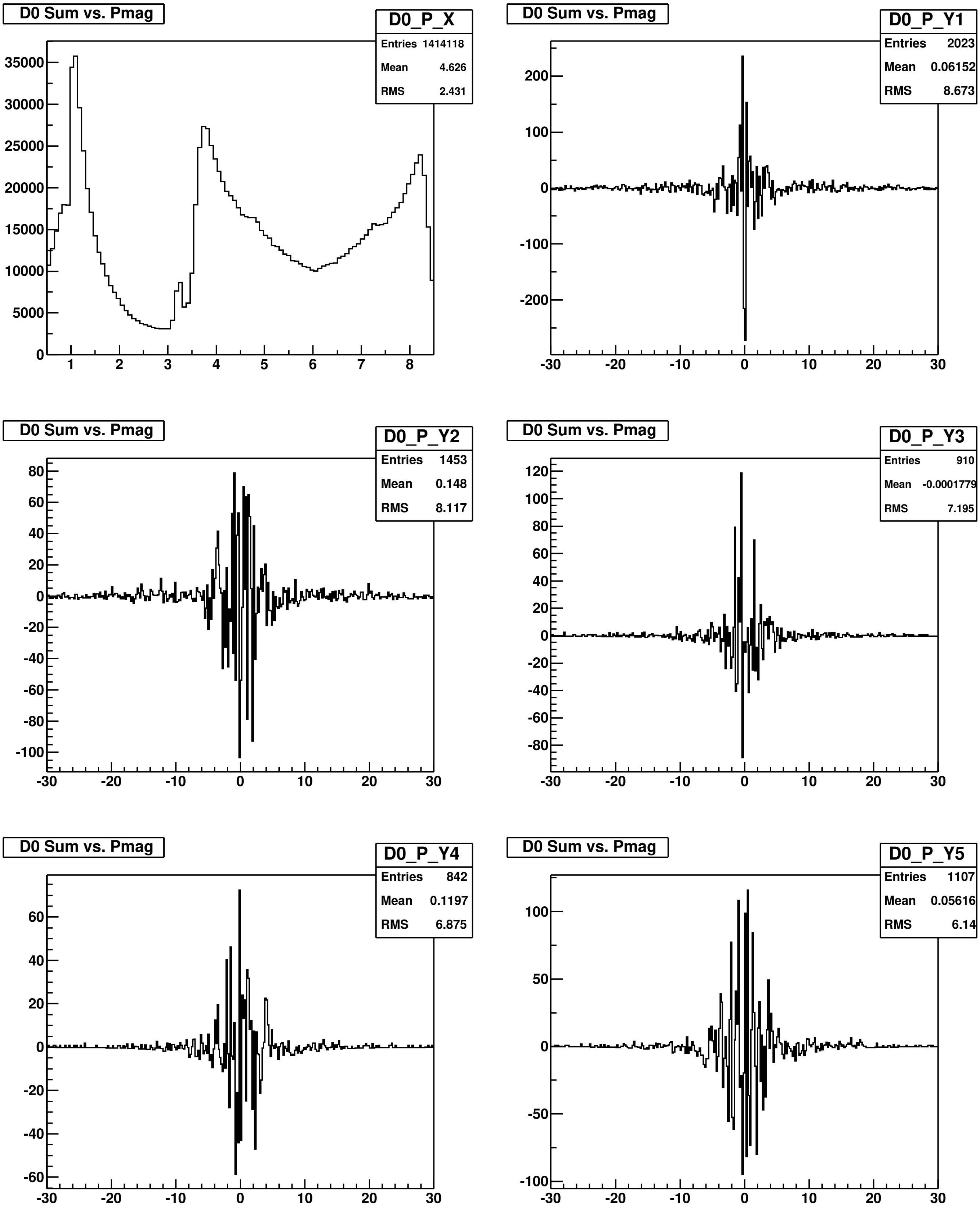

Figure 3: Residuals of d_0 Sum divided by errors as a function of momentum fit with equation 33

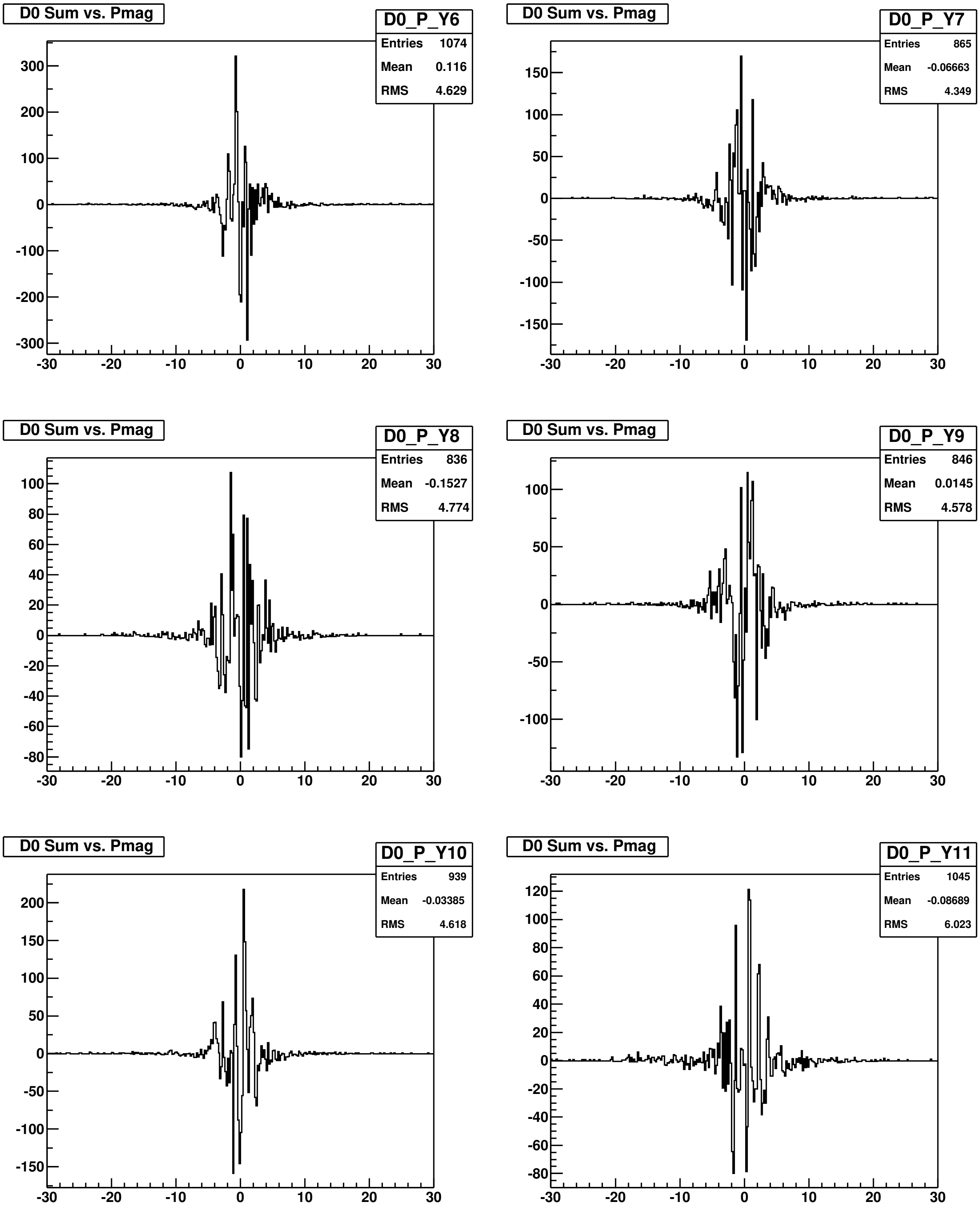

Figure 4: Residuals of d_0 Sum divided by errors as a function of momentum fit with equation 33

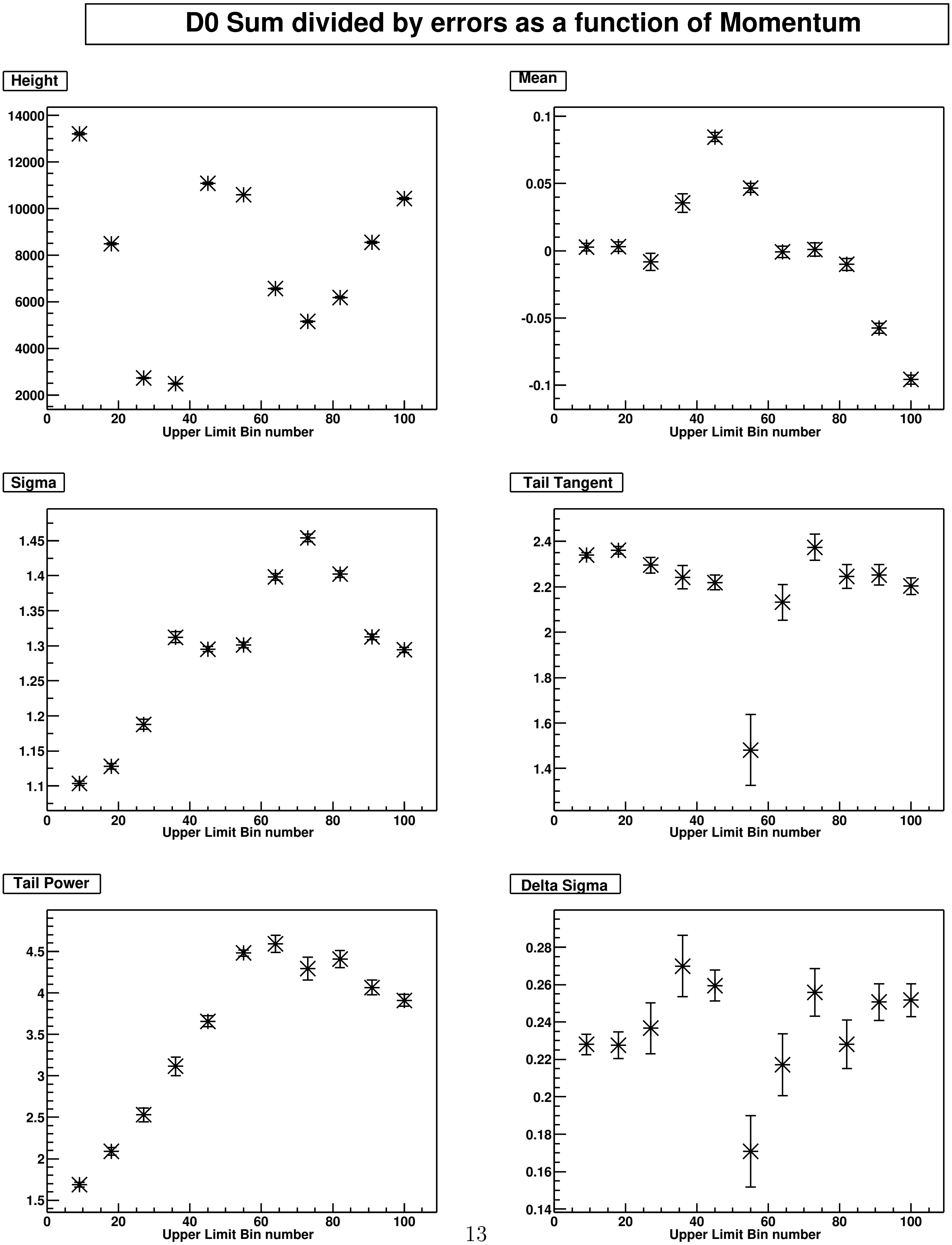

Figure 5: Parameters of equation 33 versus bin number for d_0 Sum divided by errors as a function of momentum

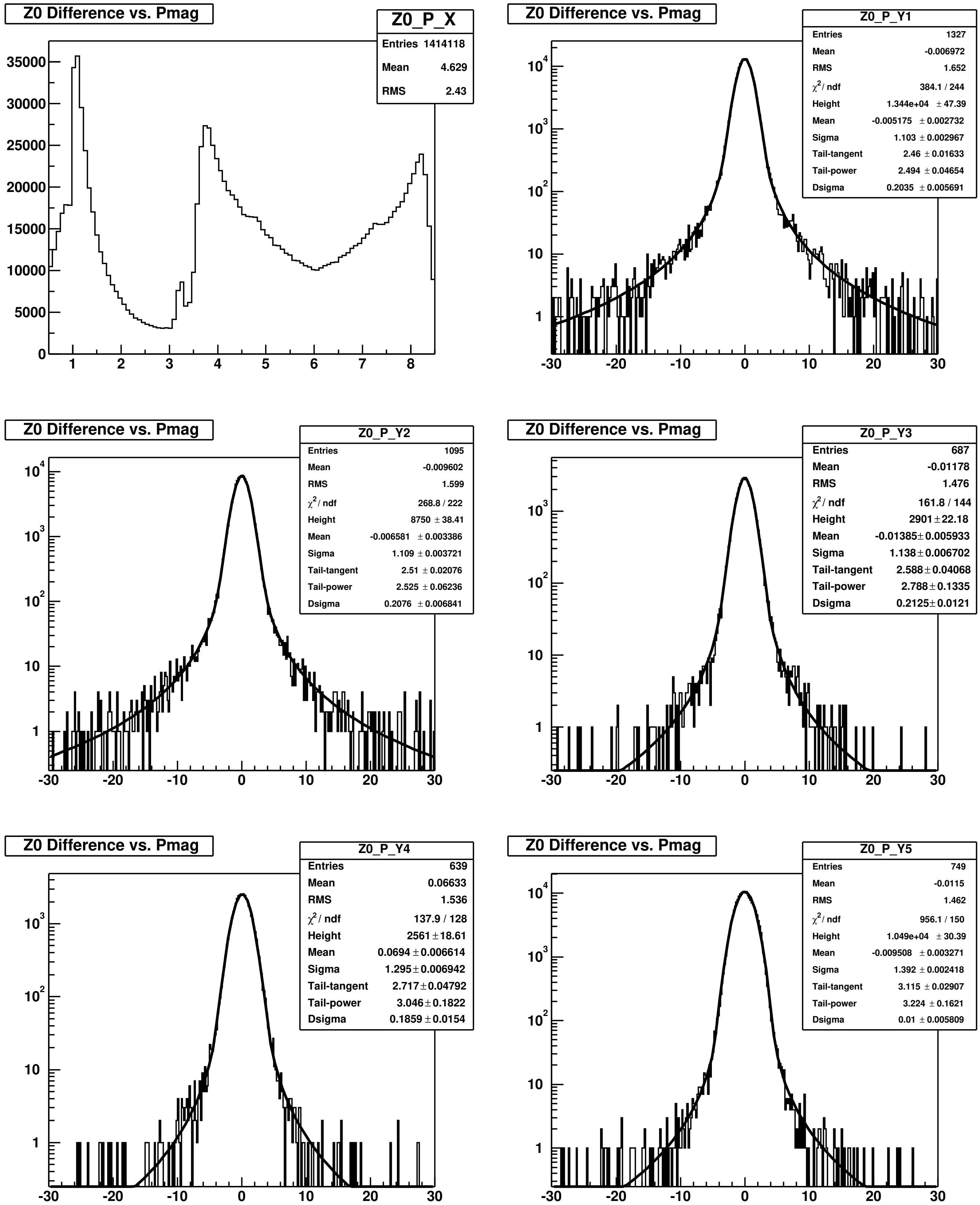

Figure 6: z_0 Difference divided by errors as a function of momentum fit with equation 33

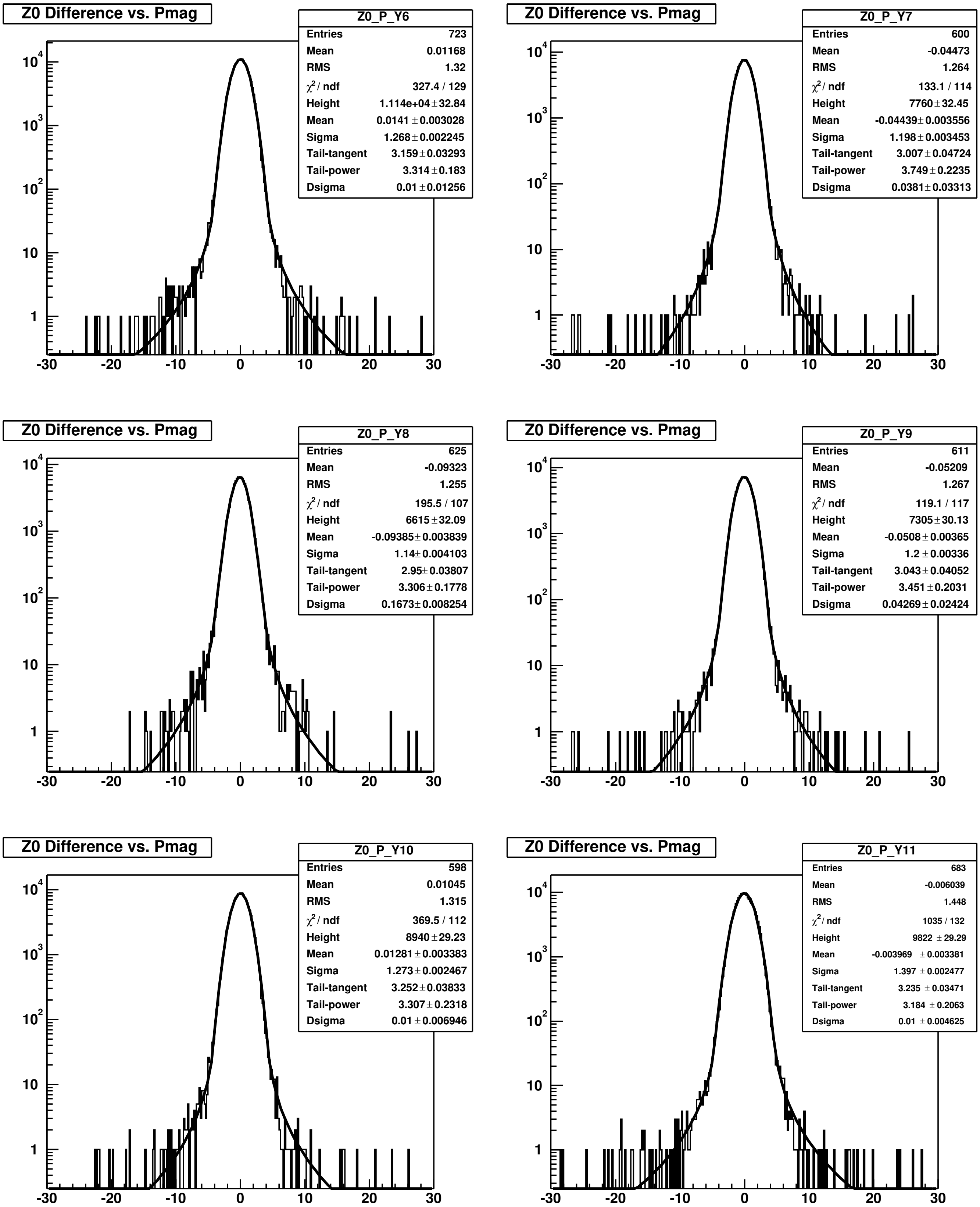

Figure 7: z_0 Difference divided by errors as a function of momentum fit with equation 33

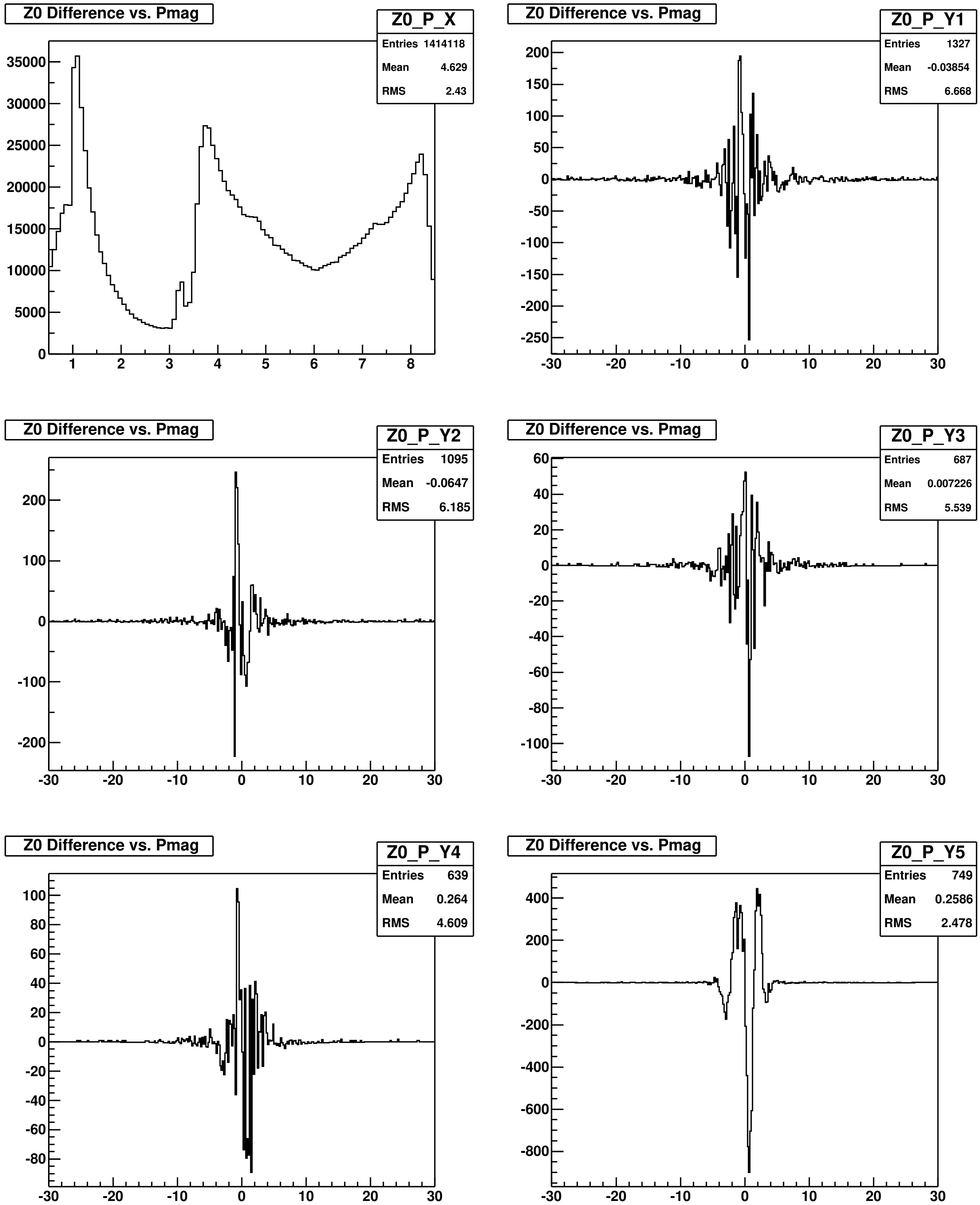

Figure 8: Residuals of z_0 Difference divided by errors as a function of momentum fit with equation 33

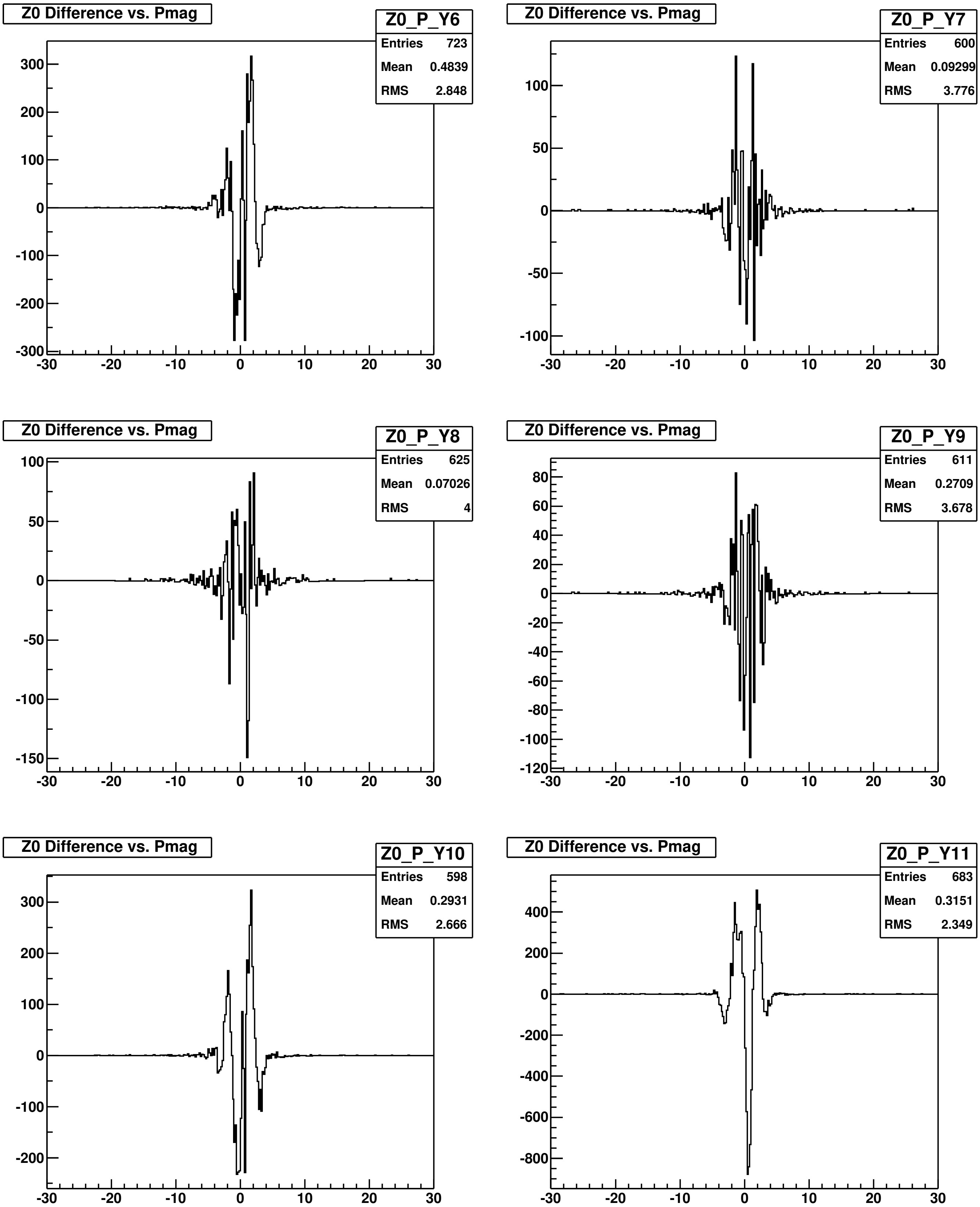

Figure 9: Residuals of z_0 Difference divided by errors as a function of momentum fit with equation 33

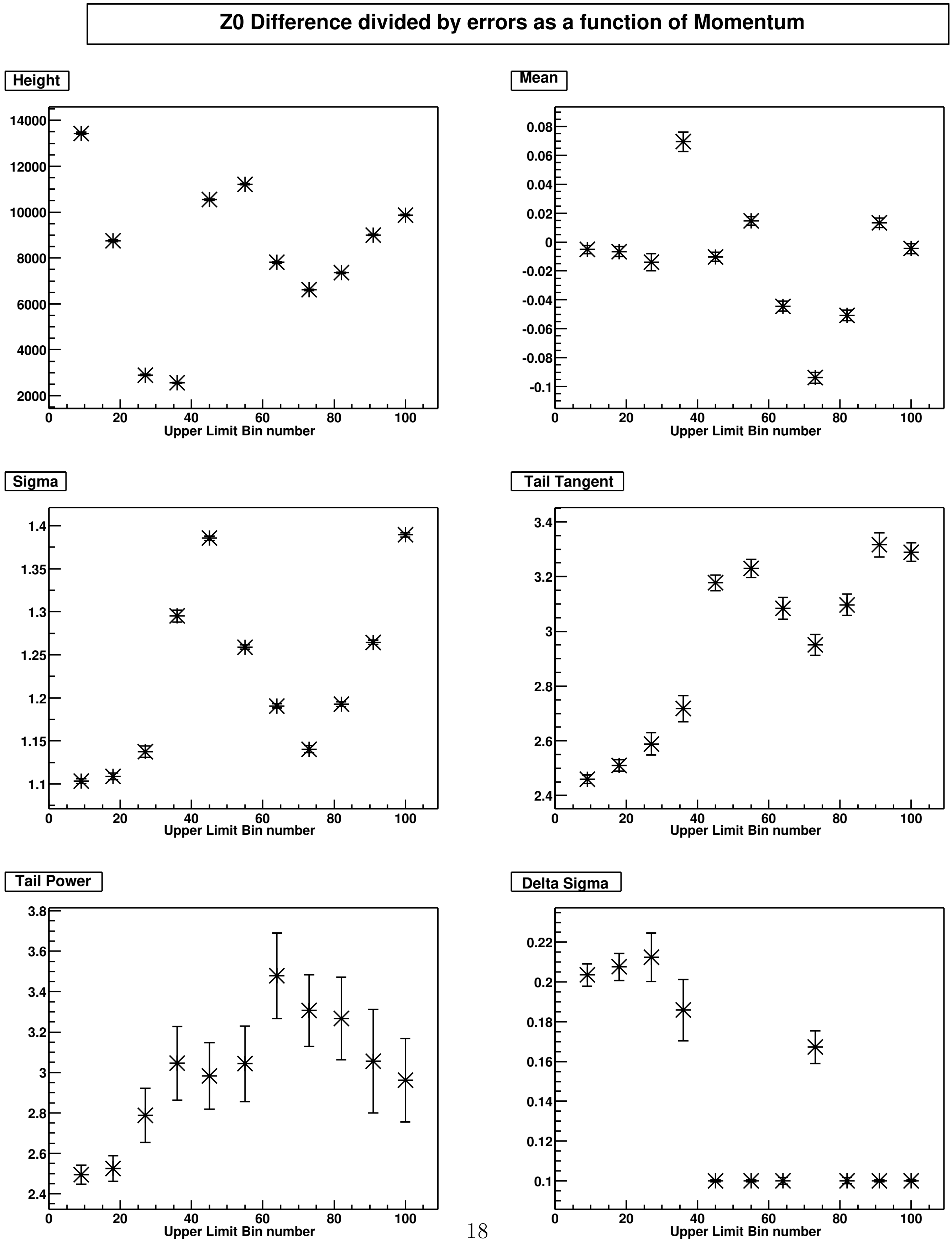

Figure 10: Parameters of equation 33 versus bin number for z_0 Difference divided by errors as a function of momentum

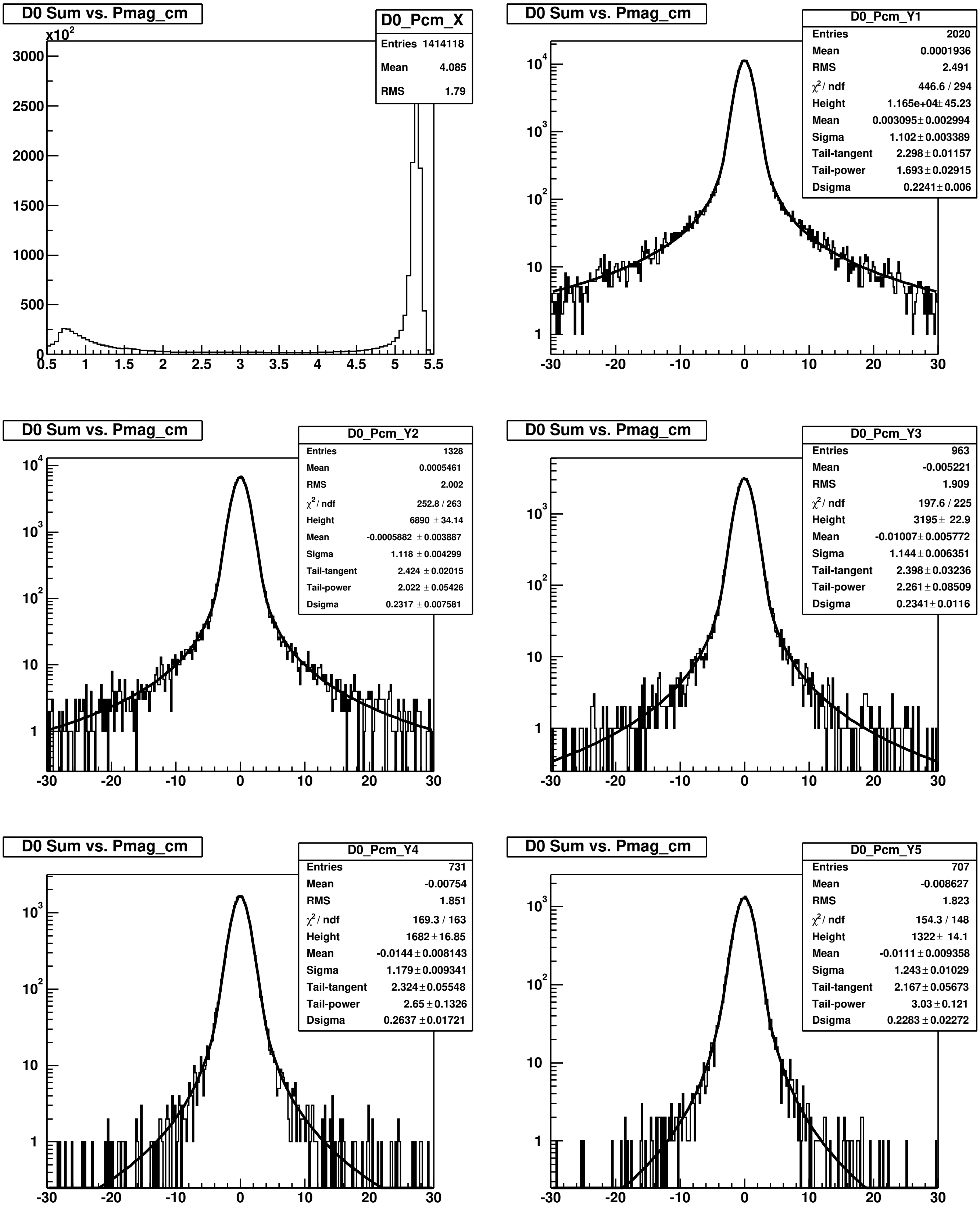

Figure 11: d_0 Sum divided by errors as a function of center-of-mass momentum fit with equation 33

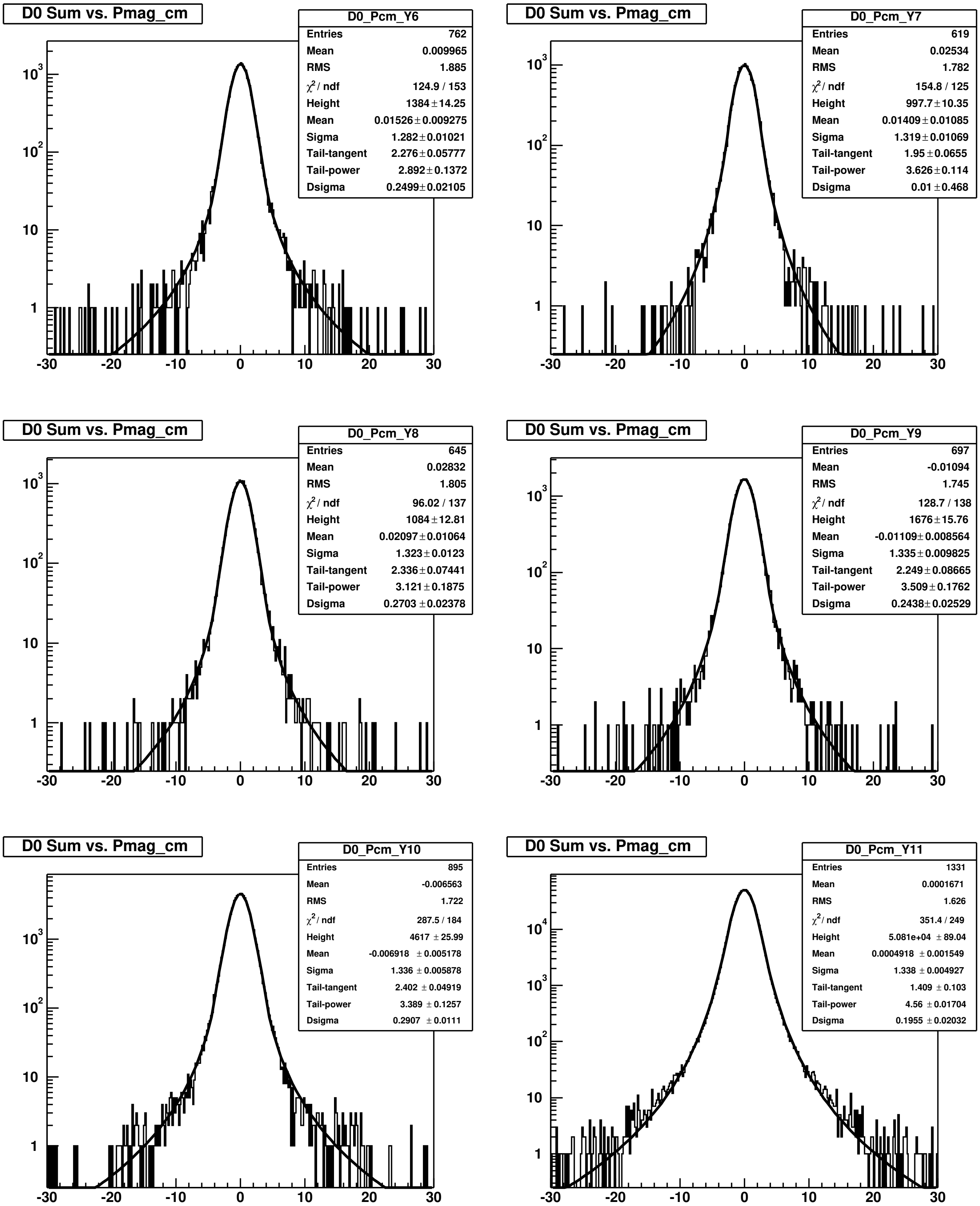

Figure 12: d_0 Sum divided by errors as a function of center-of-mass momentum fit with equation 33

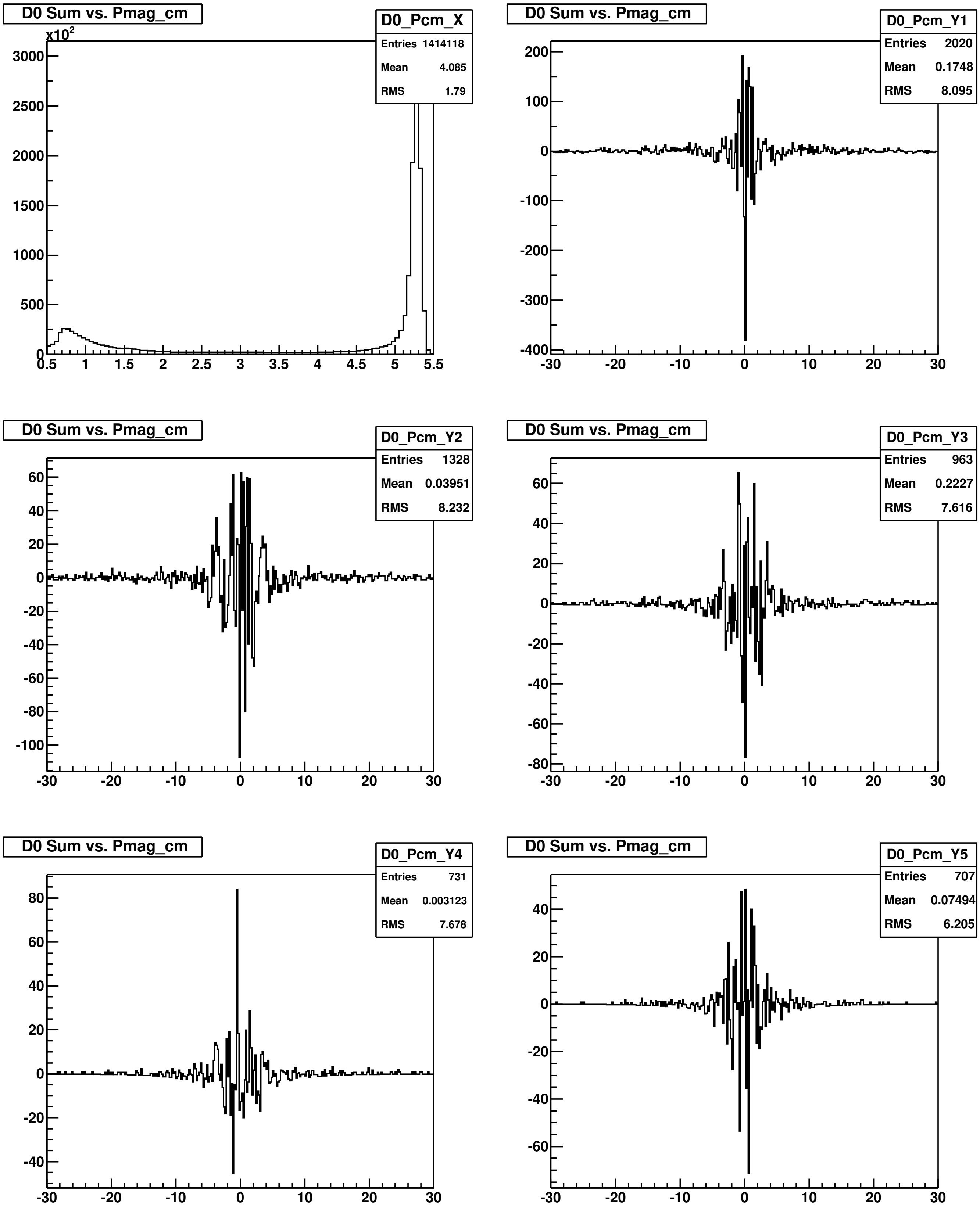

Figure 13: Residuals of d_0 Sum divided by errors as a function of center-of-mass momentum fit with equation 33

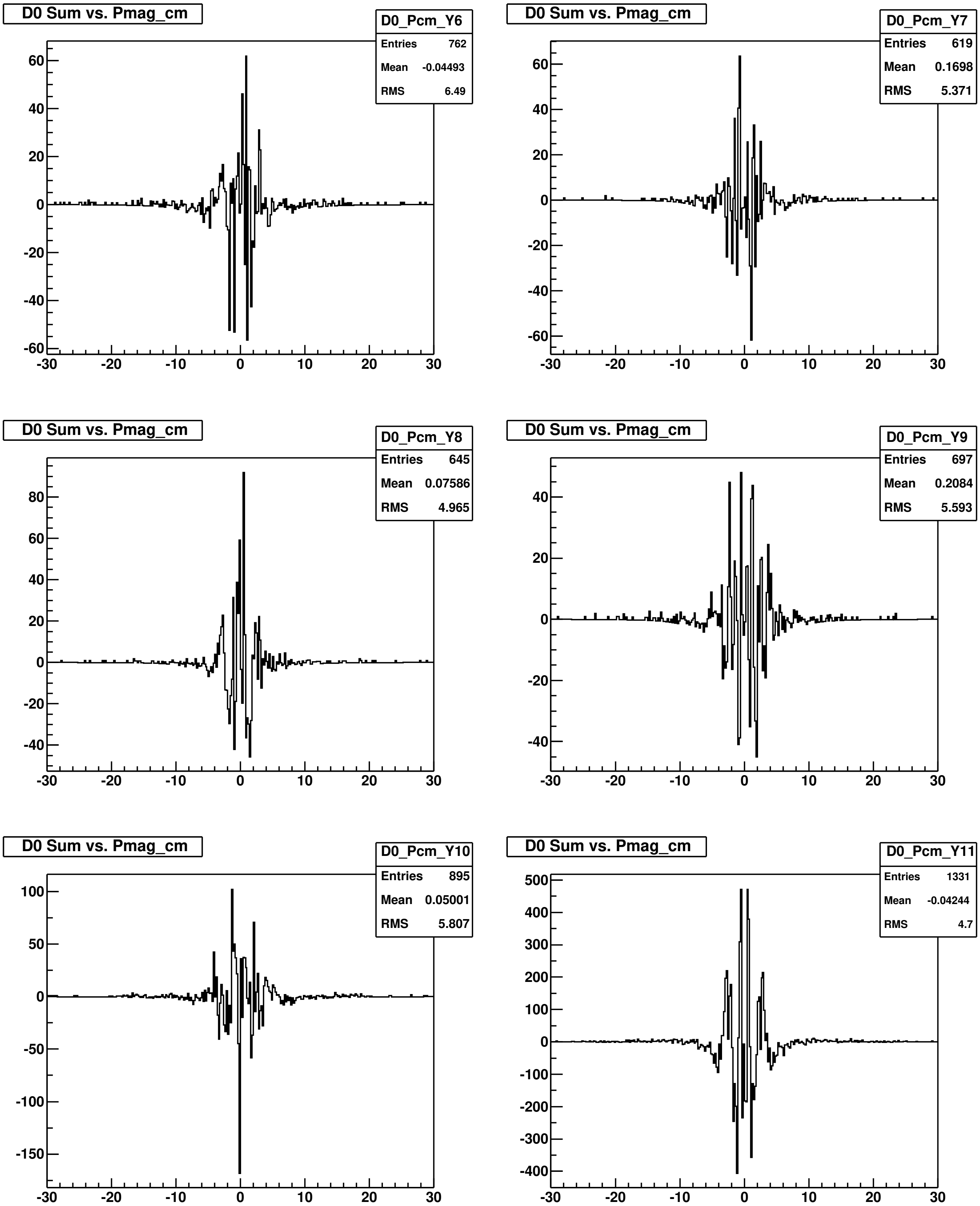

Figure 14: Residuals of d_0 Sum divided by errors as a function of center-of-mass momentum fit with equation 33

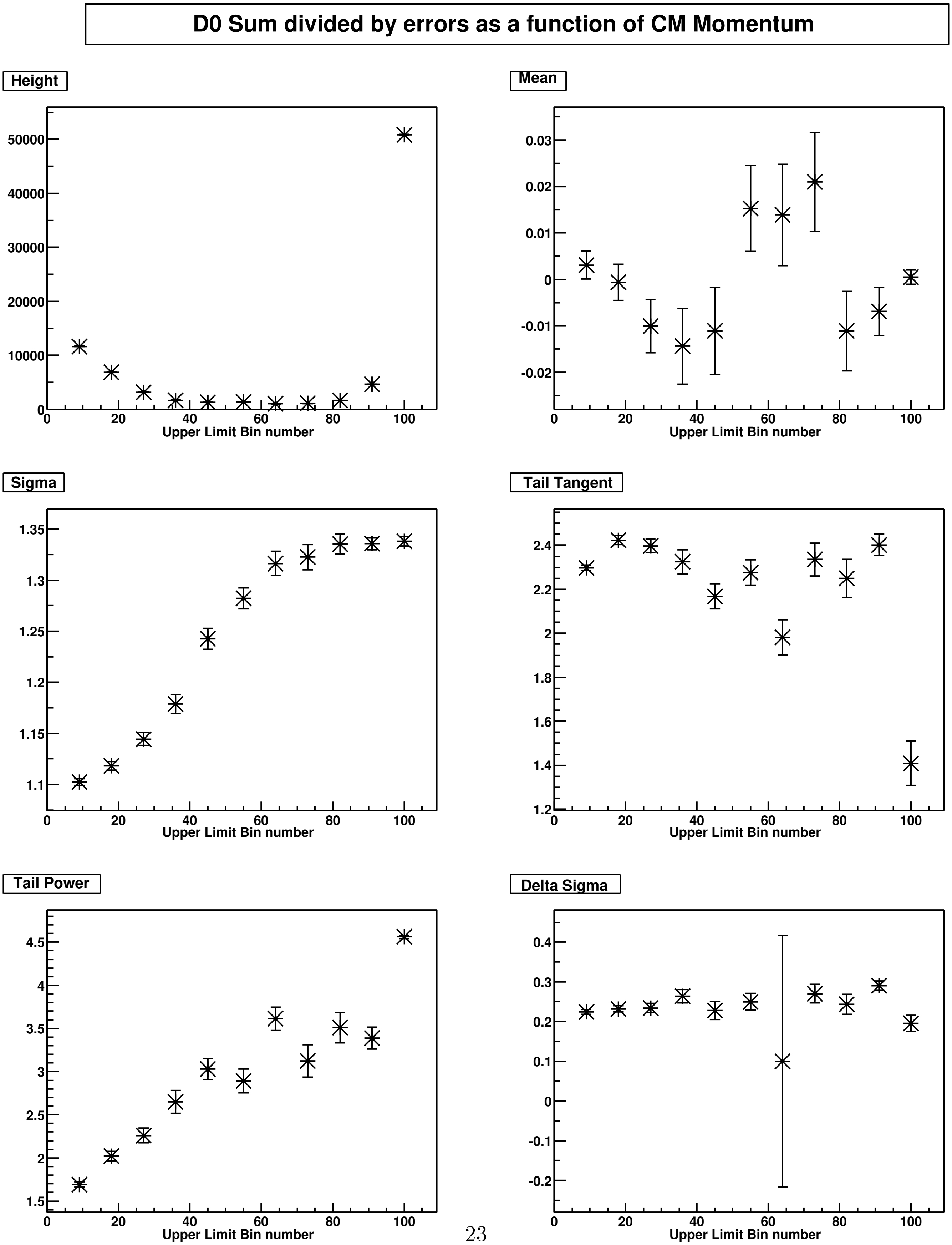

Figure 15: Parameters of equation 33 versus bin number for d_0 Sum divided by errors as a function of center-of-mass momentum

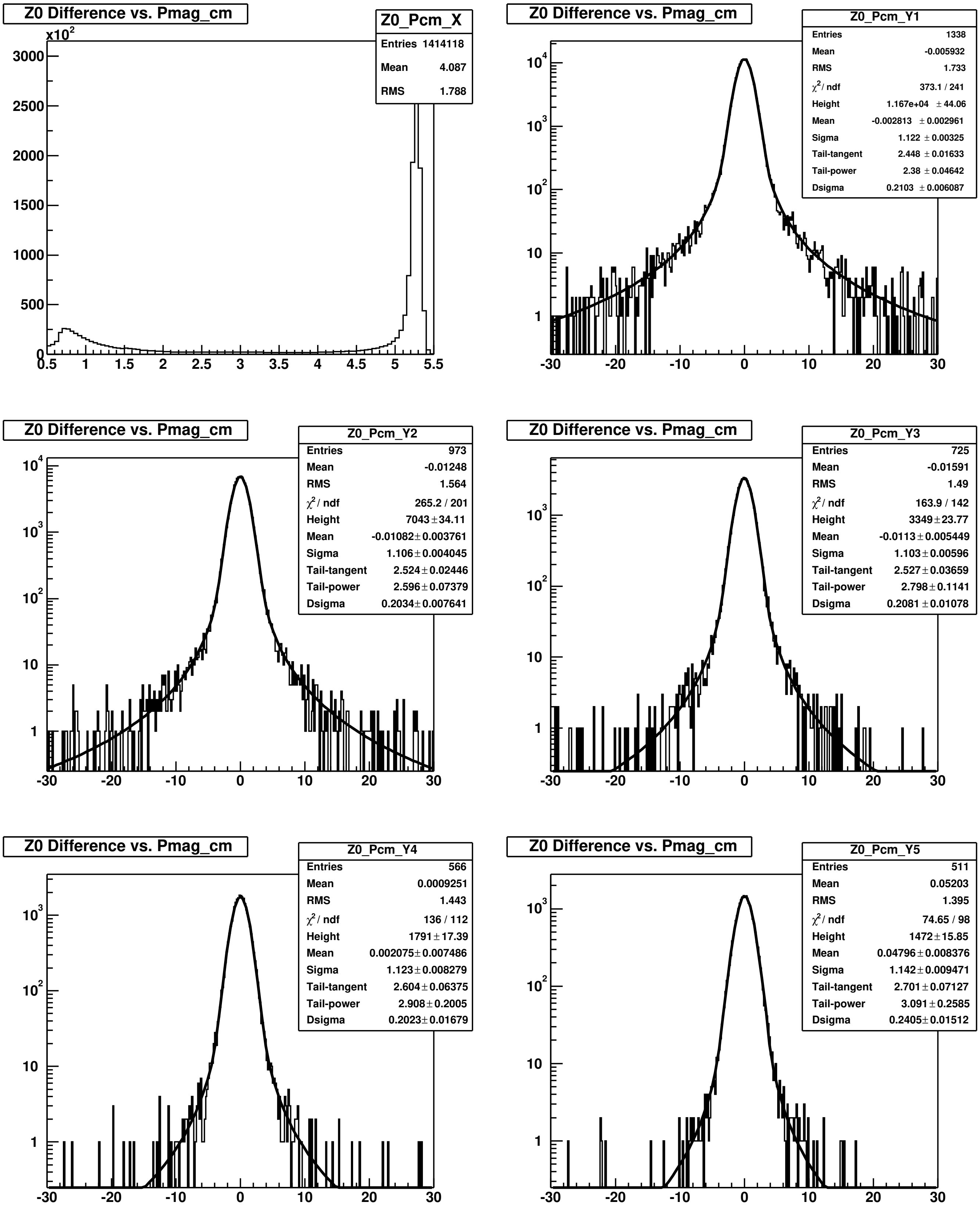

Figure 16: z_0 Difference divided by errors as a function of center-of-mass momentum fit with equation 33

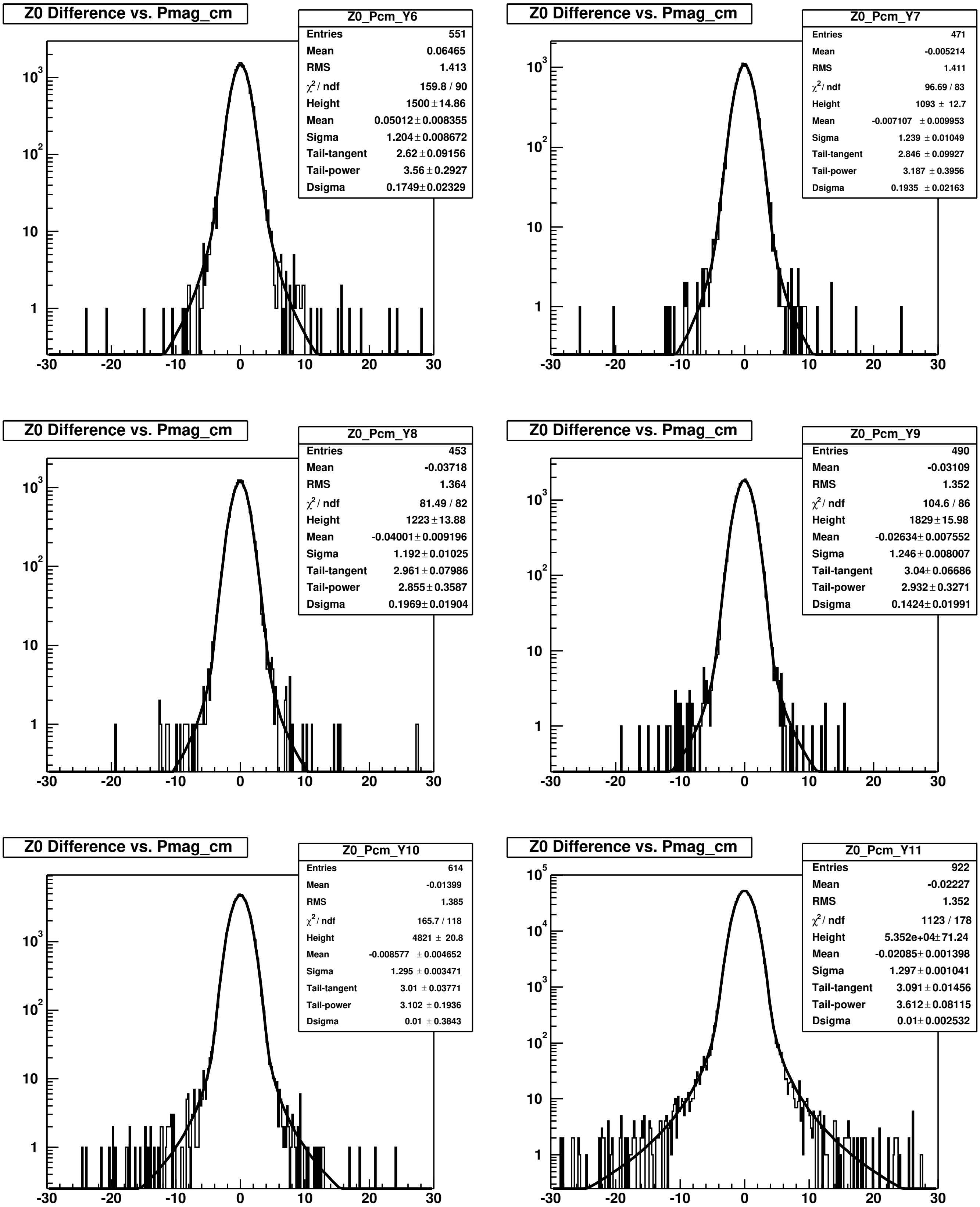

Figure 17: z_0 Difference divided by errors as a function of center-of-mass momentum fit with equation 33

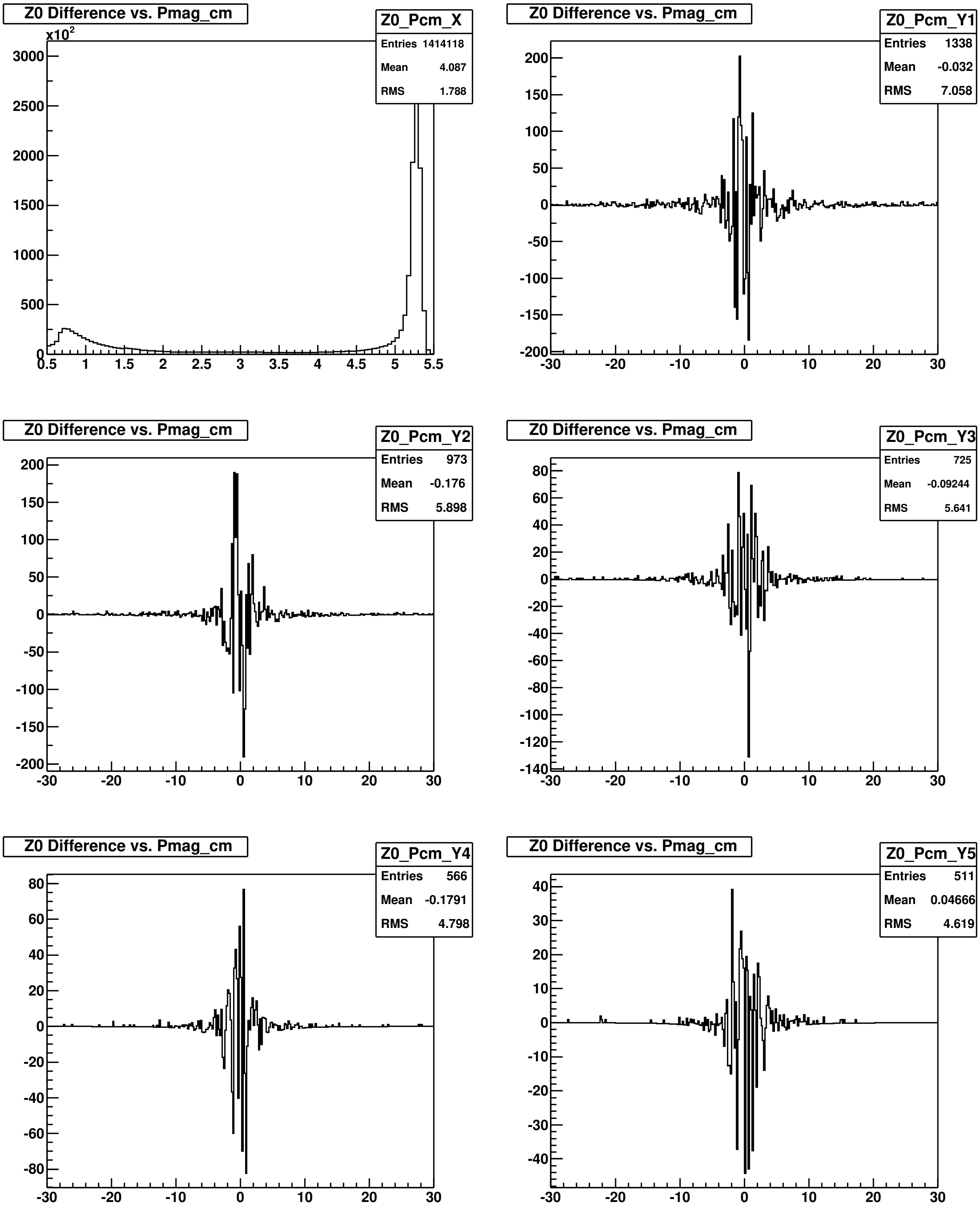

Figure 18: Residuals of z_0 Difference divided by errors as a function of center-of-mass momentum fit with equation 33

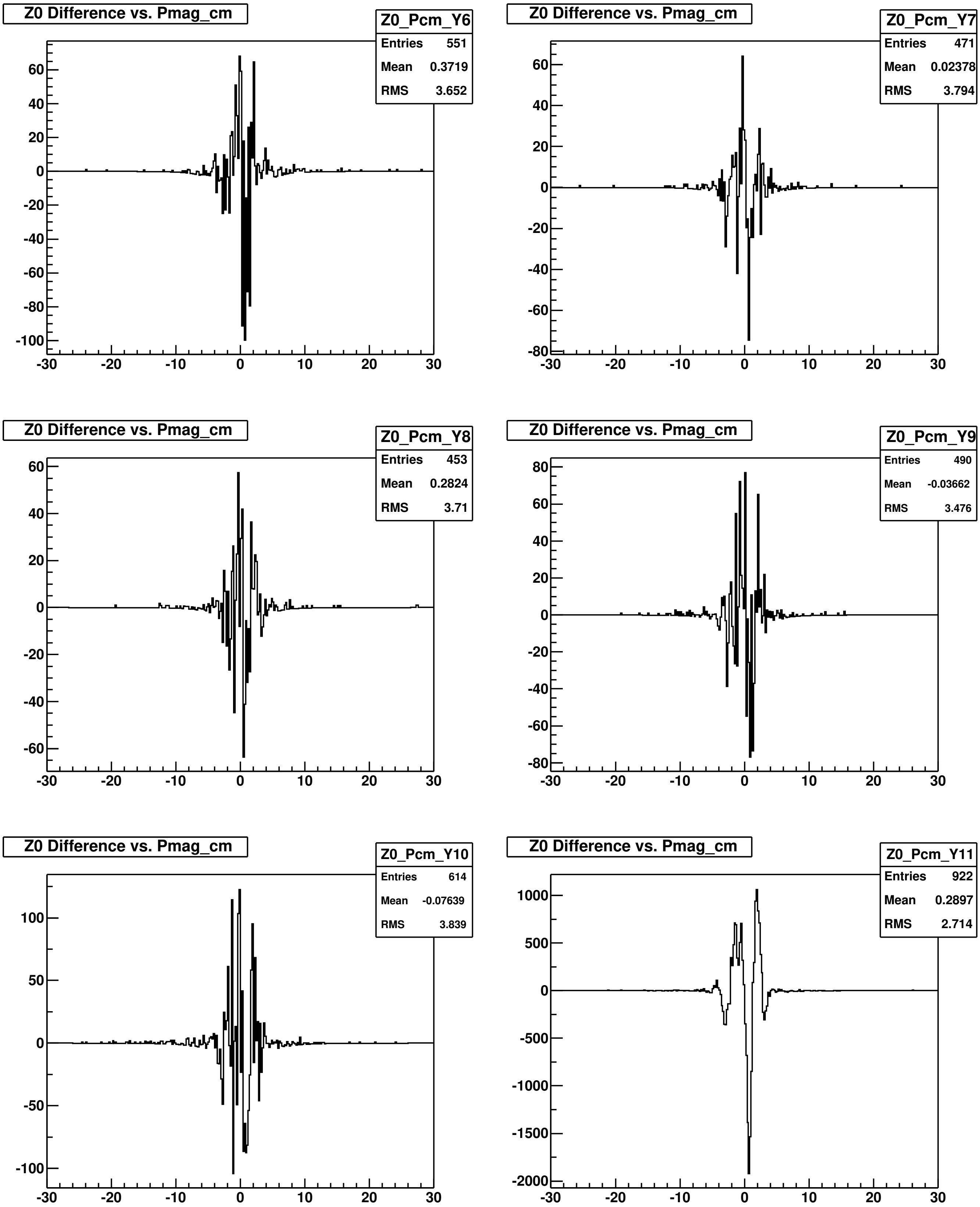

Figure 19: Residuals of z_0 Difference divided by errors as a function of center-of-mass momentum fit with equation 33

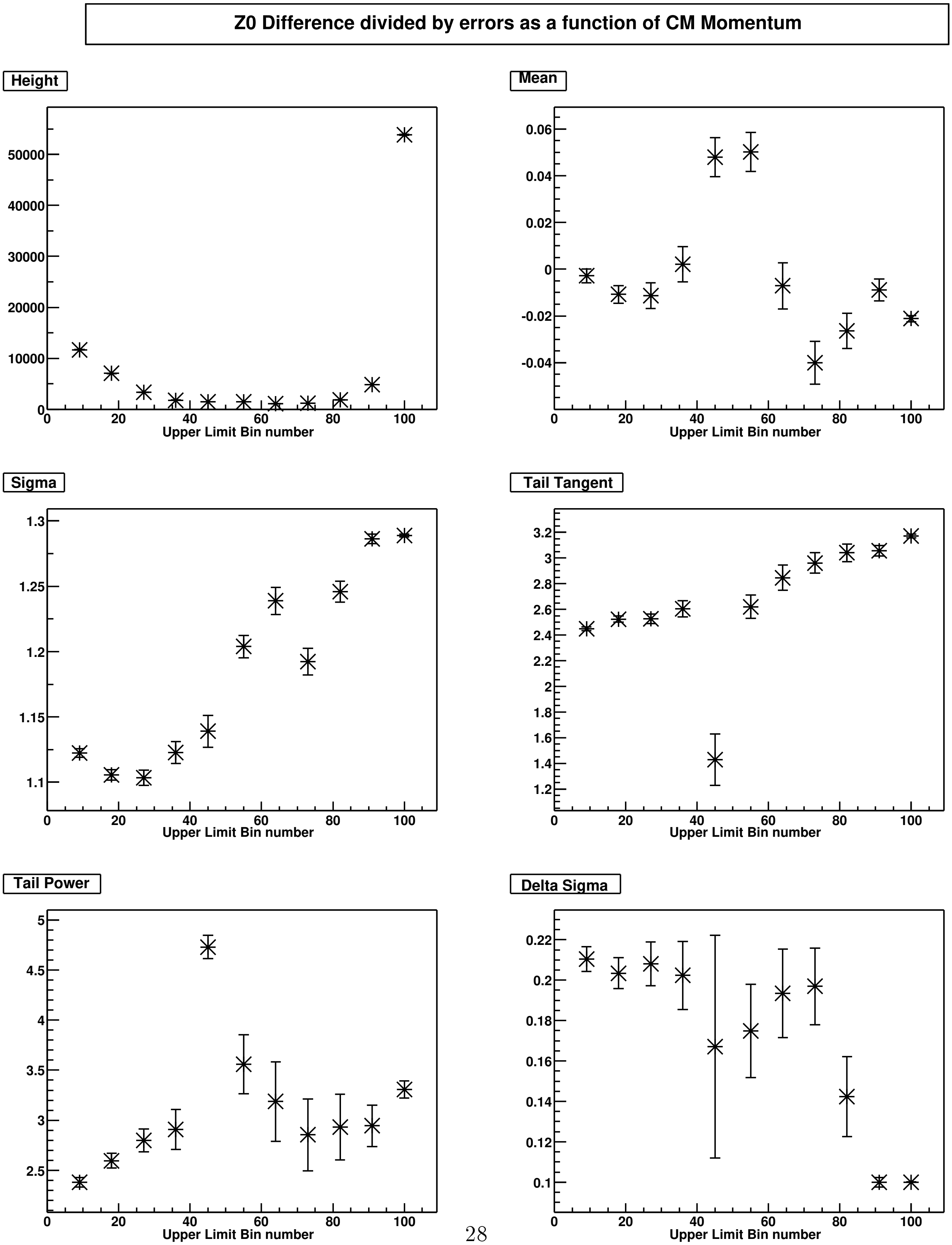

Figure 20: Parameters of equation 33 versus bin number for z_0 Difference divided by errors as a function of center-of-mass momentum

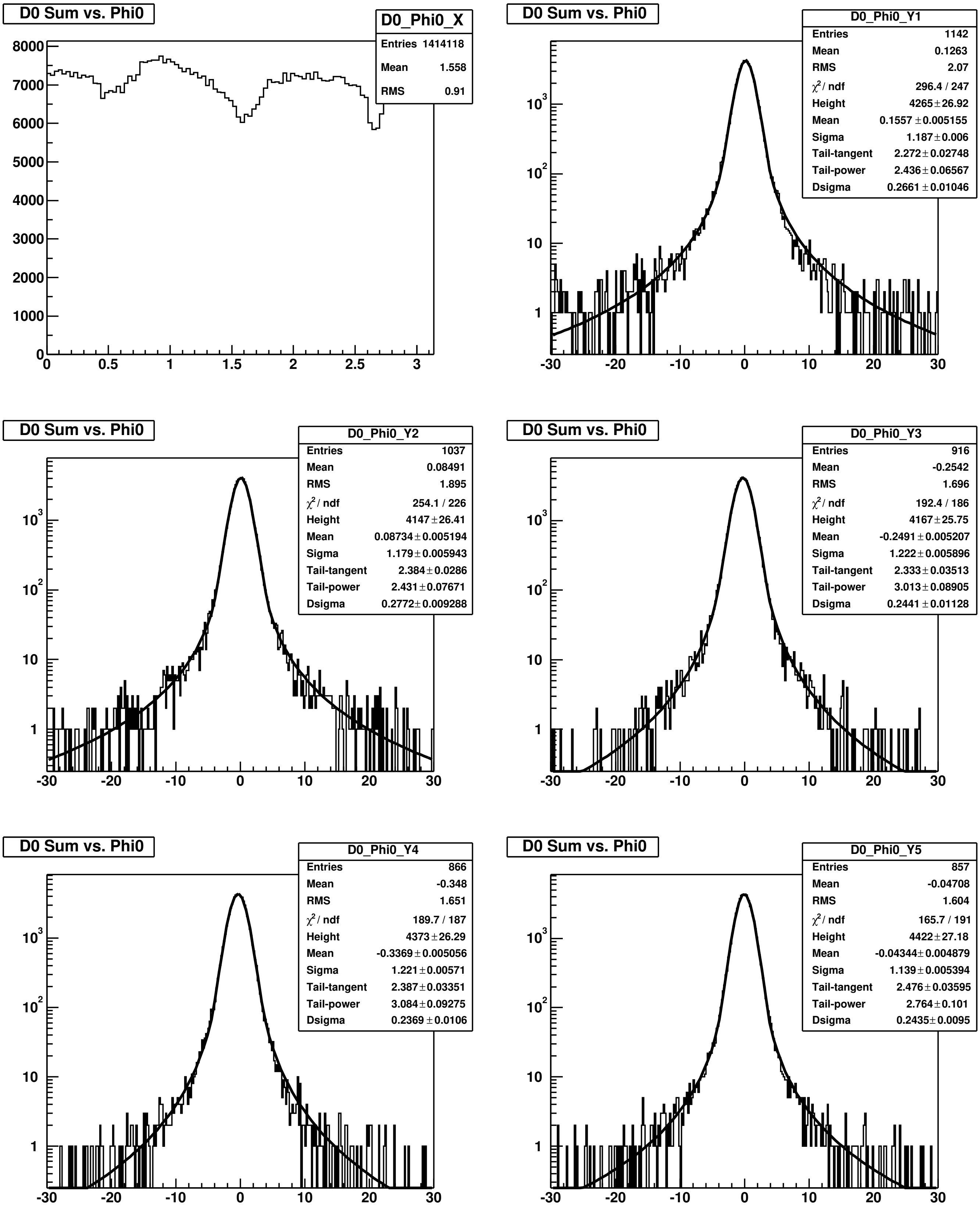

Figure 21: d_0 Sum divided by errors as a function of ϕ_0 fit with equation 33

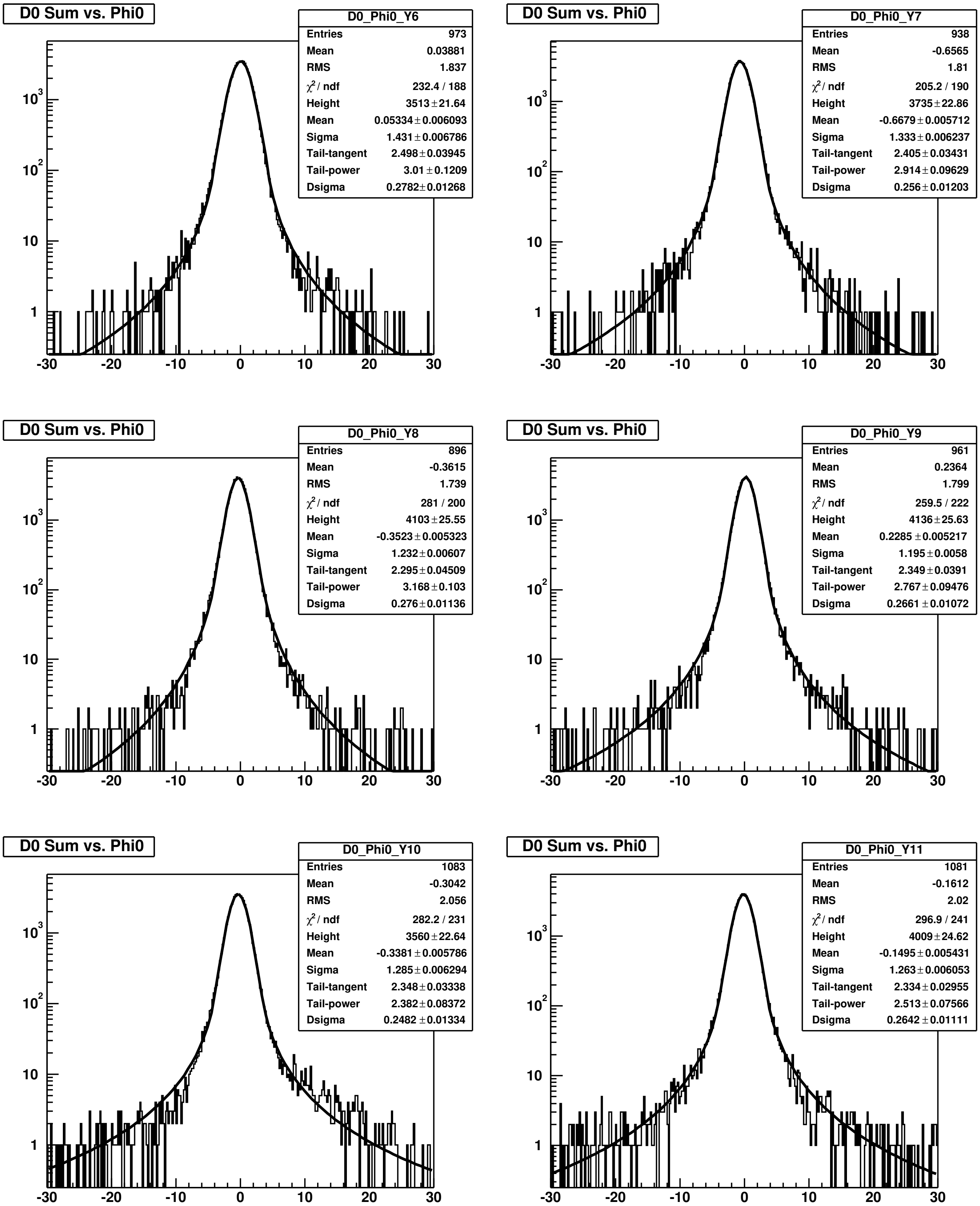

Figure 22: d_0 Sum divided by errors as a function of ϕ_0 fit with equation 33

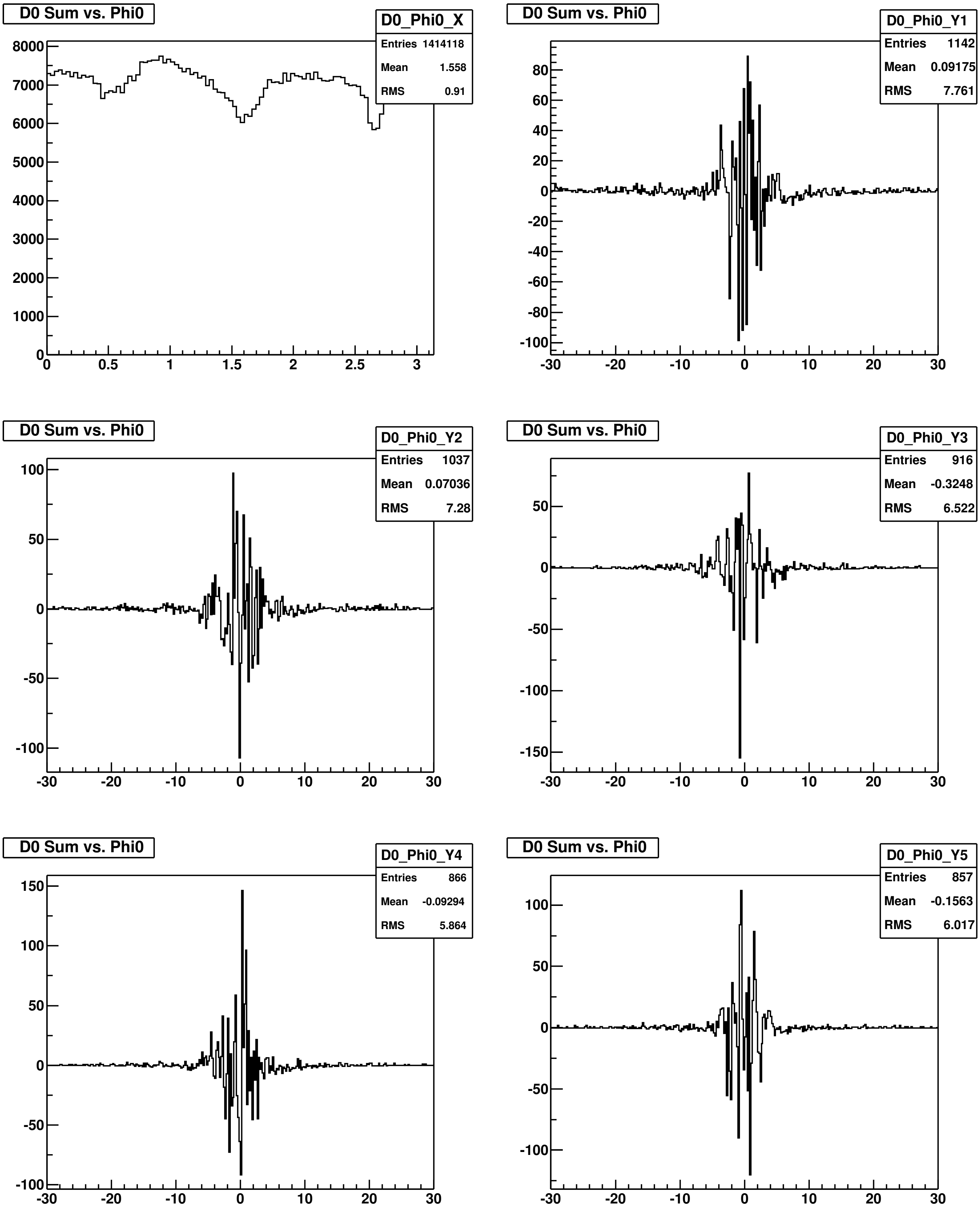

Figure 23: Residuals of d_0 Sum divided by errors as a function of ϕ_0 fit with equation 33

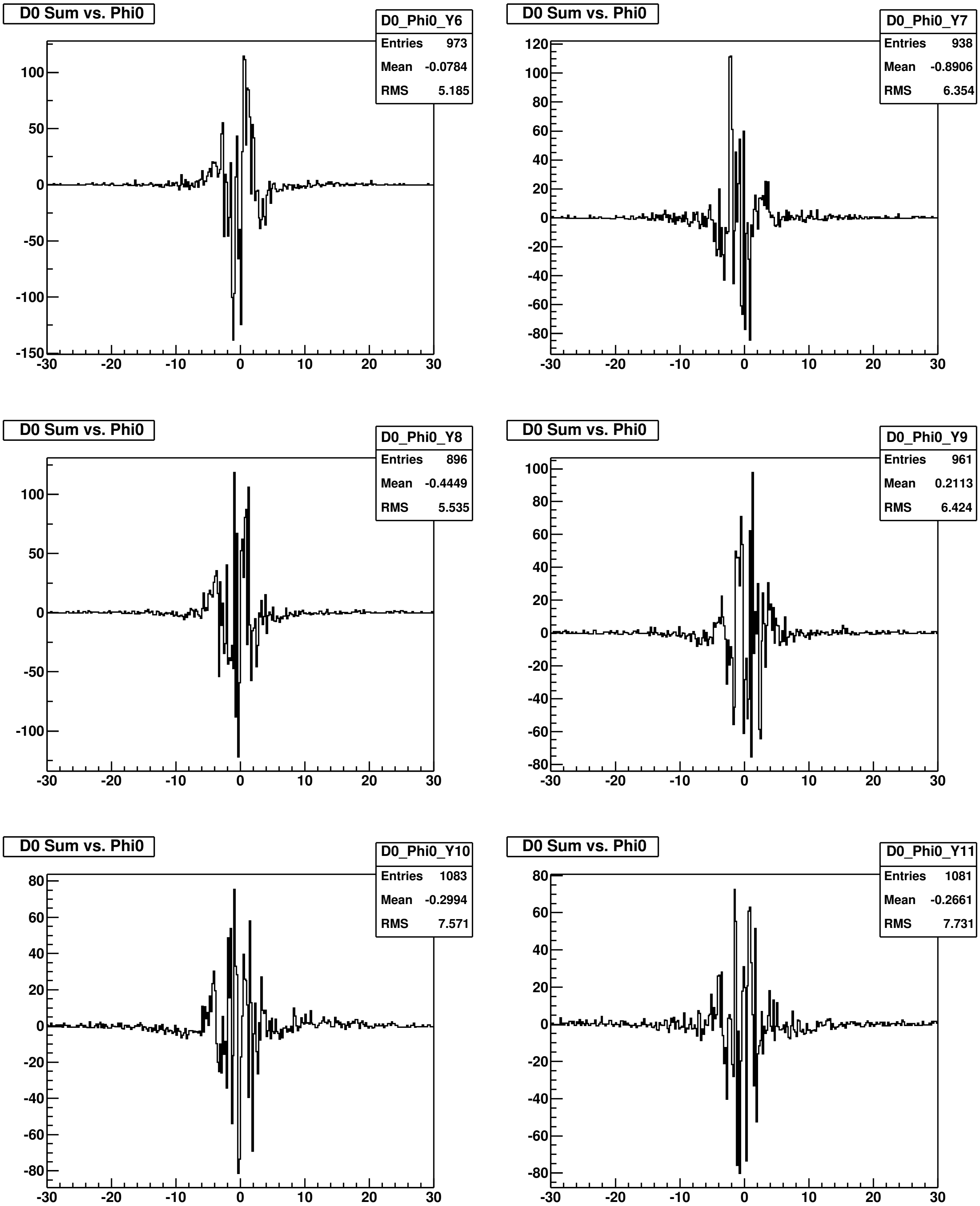

Figure 24: Residuals of d_0 Sum divided by errors as a function of ϕ_0 fit with equation 33

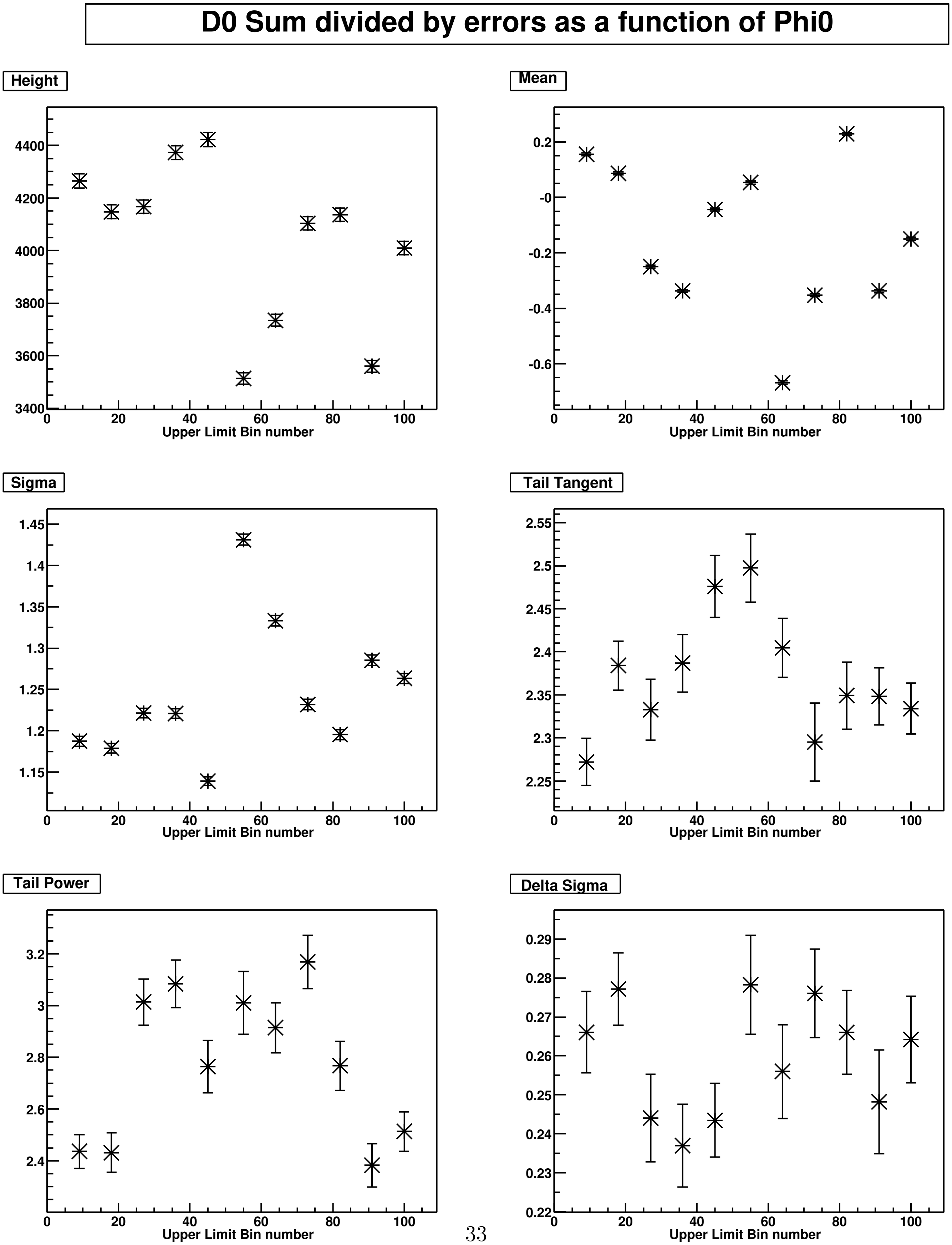

Figure 25: Parameters of equation 33 versus bin number for d_0 Sum divided by errors as a function of ϕ_0

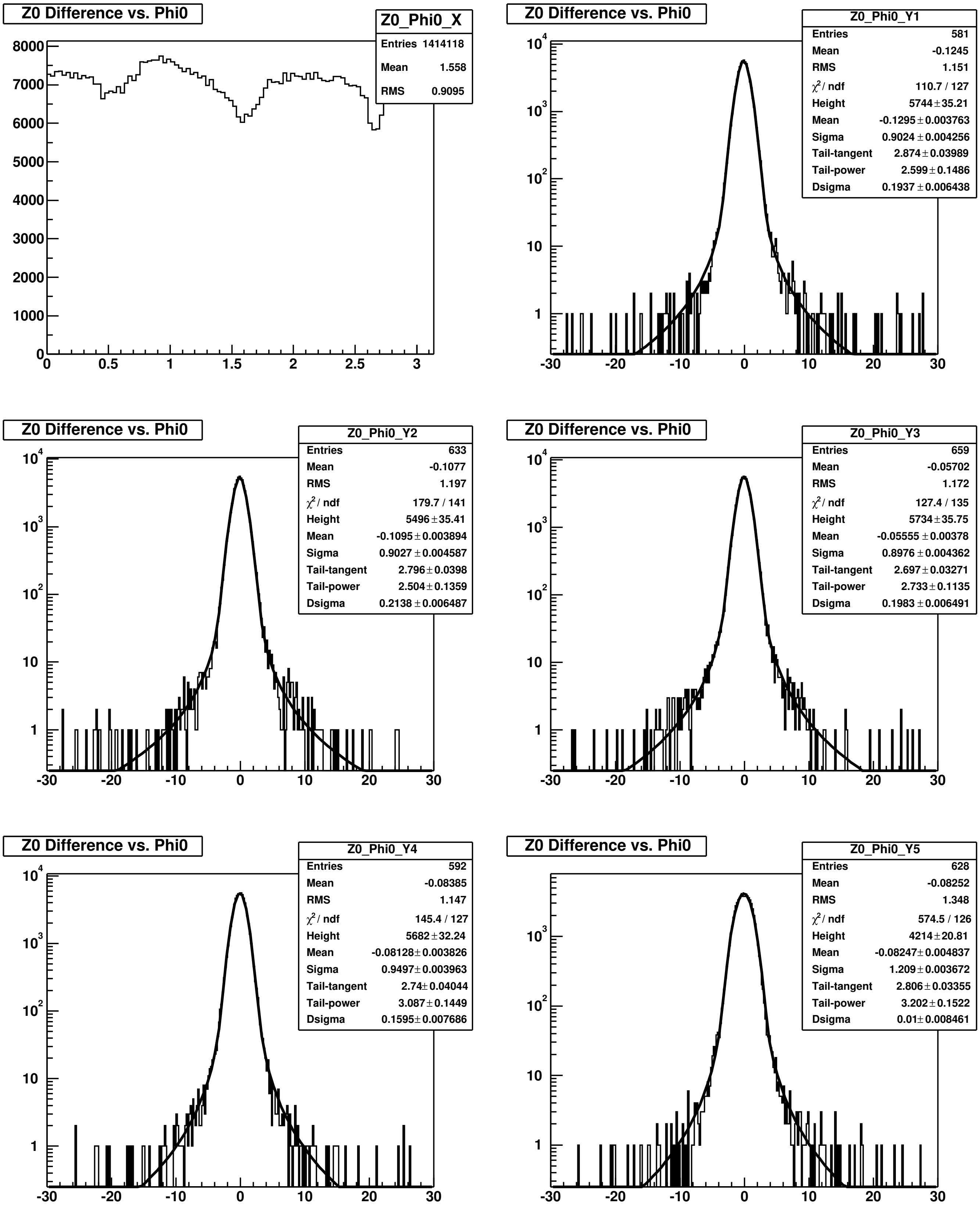

Figure 26: z_0 Difference divided by errors as a function of ϕ_0 fit with equation 33

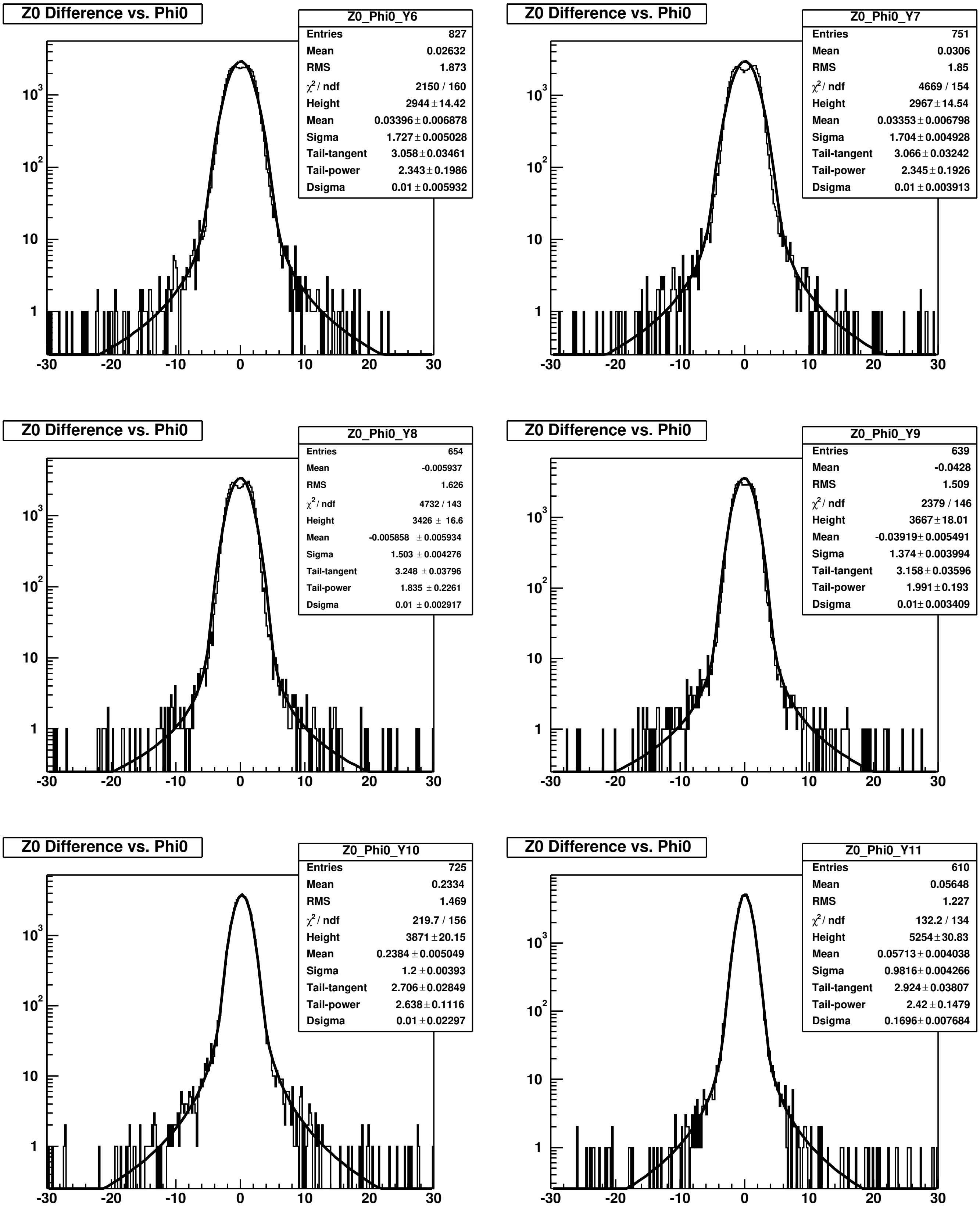

Figure 27: z_0 Difference divided by errors as a function of ϕ_0 fit with equation 33

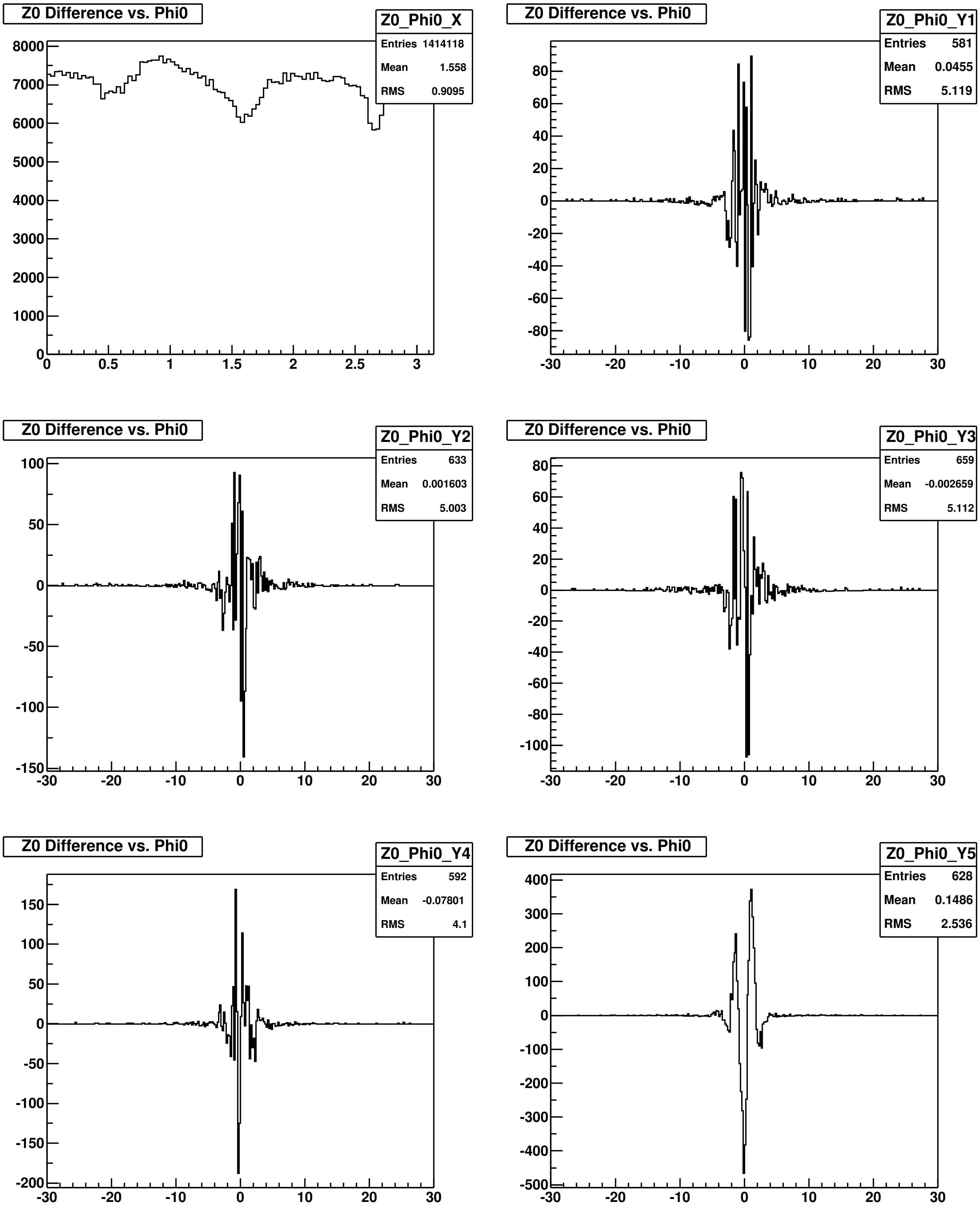

Figure 28: Residuals of z_0 Difference divided by errors as a function of ϕ_0 fit with equation 33

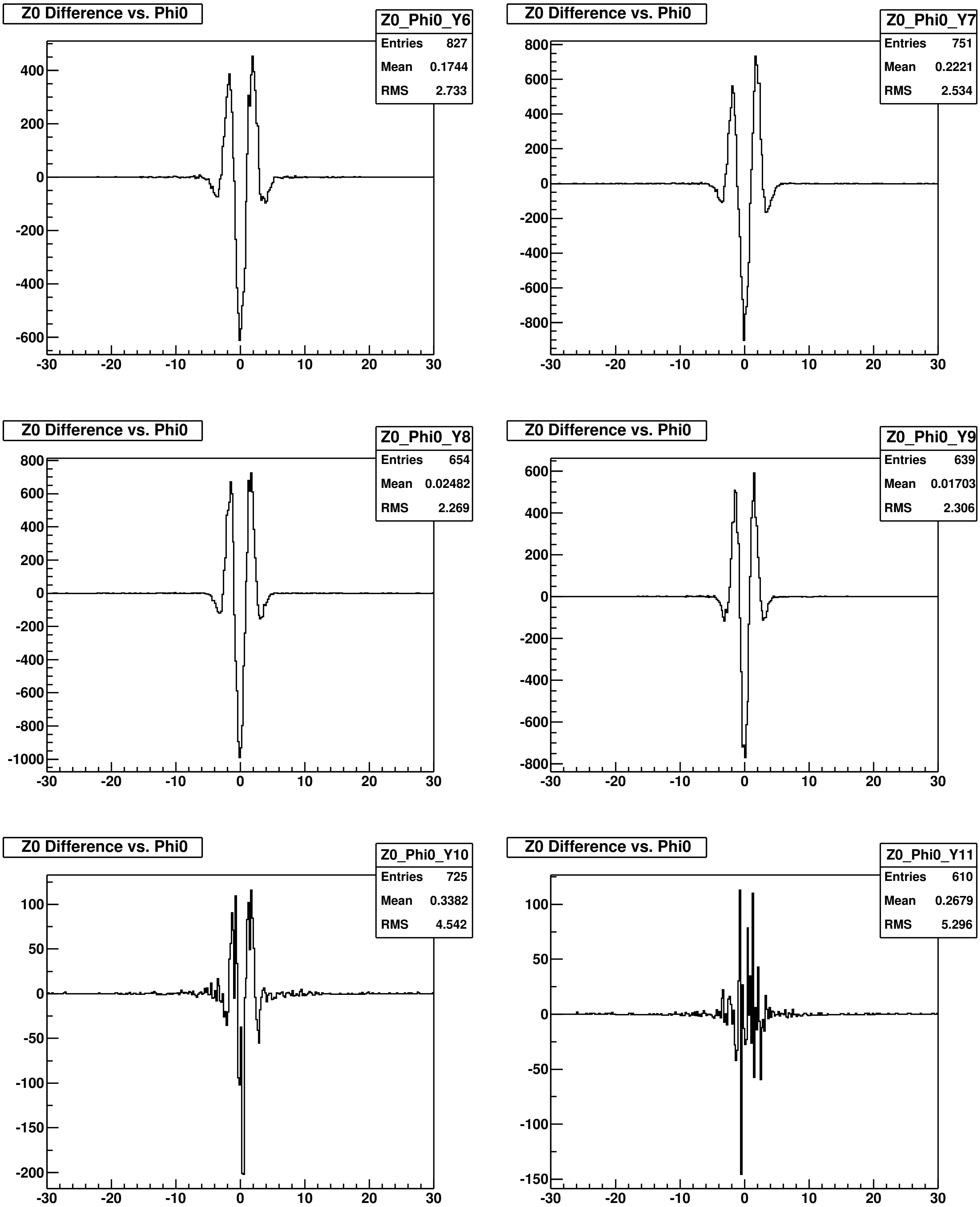

Figure 29: Residuals of z_0 Difference divided by errors as a function of ϕ_0 fit with equation 33

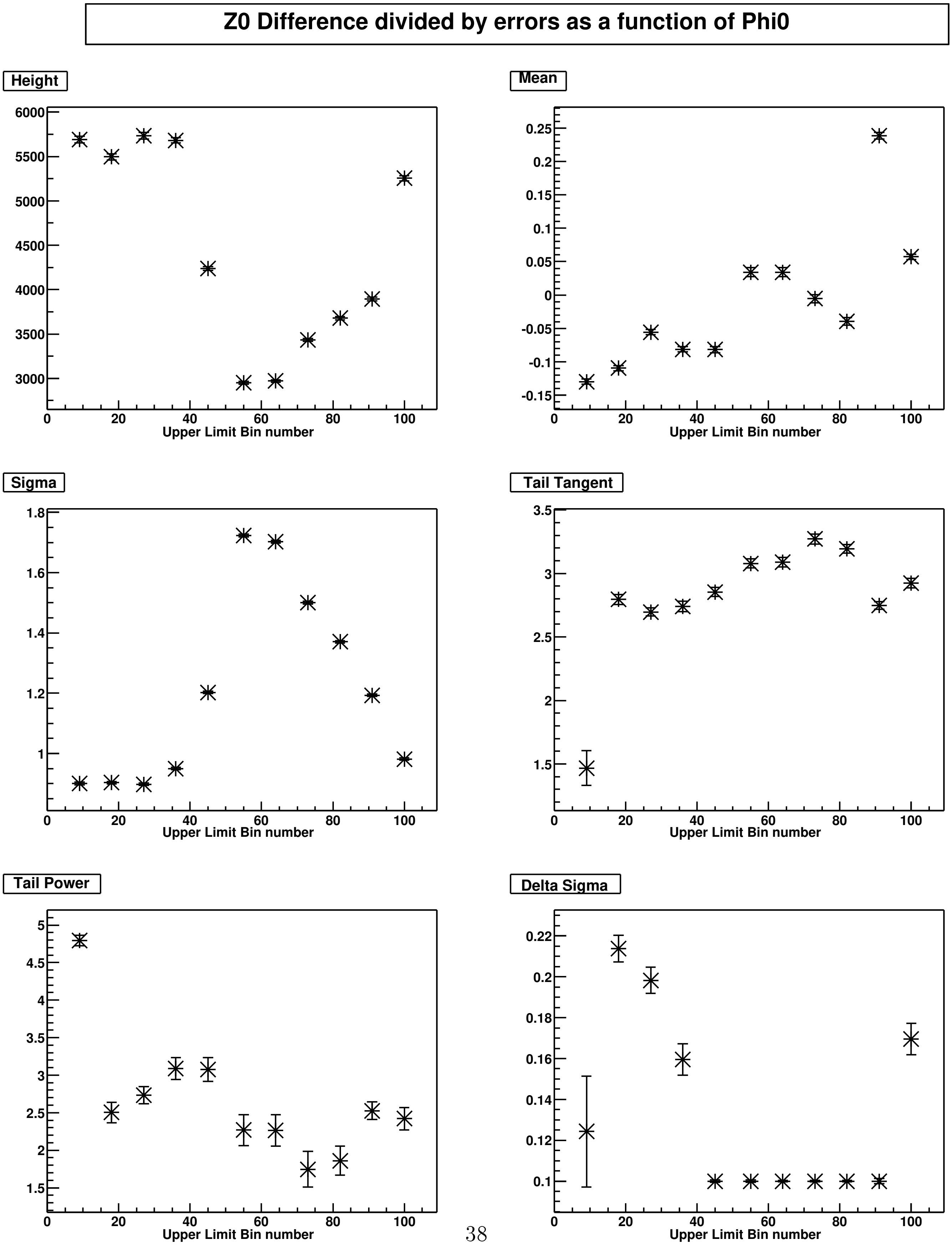

Figure 30: Parameters of equation 33 versus bin number for z_0 Difference divided by errors as a function of ϕ_0

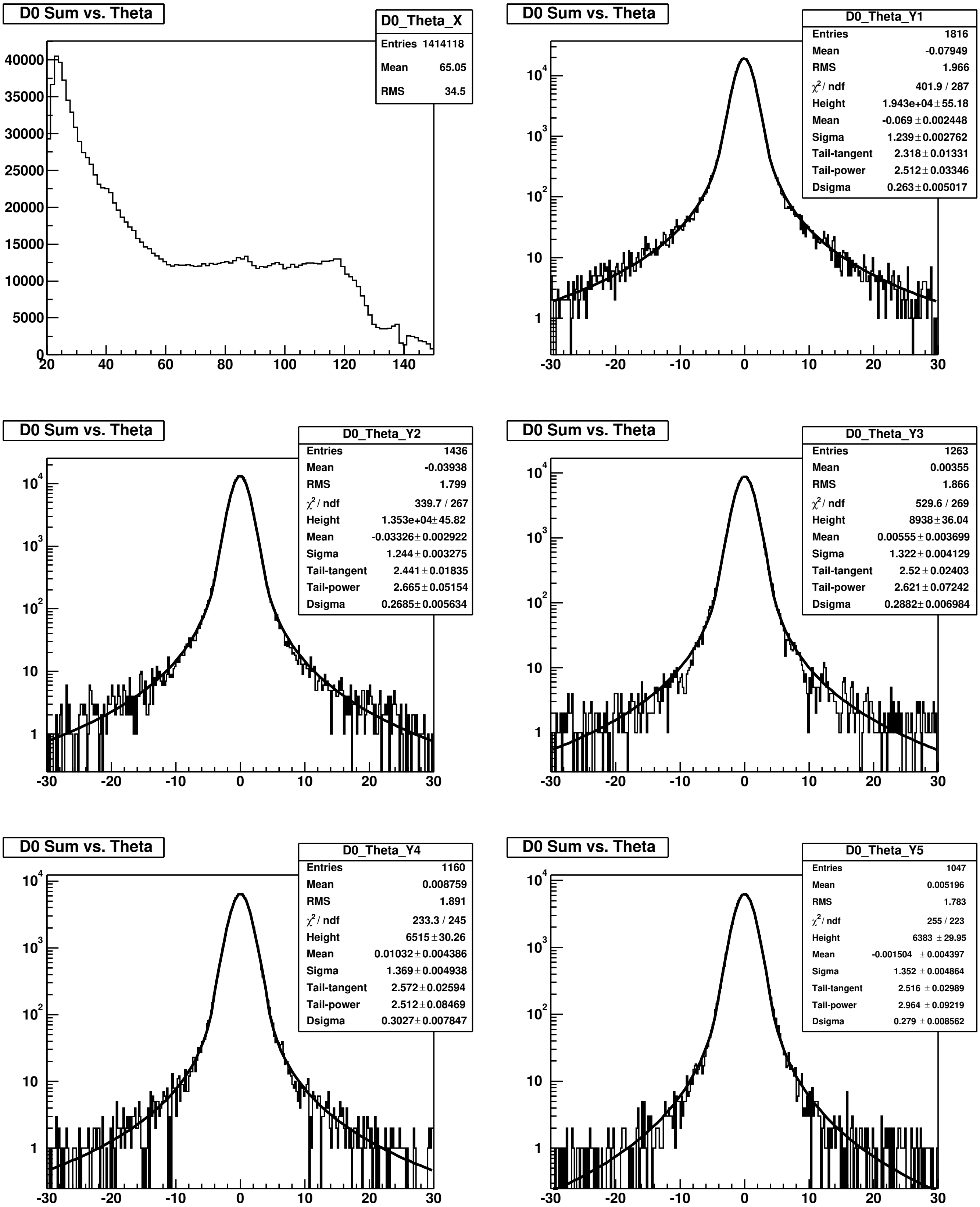

Figure 31: d_0 Sum divided by errors as a function of θ fit with equation 33

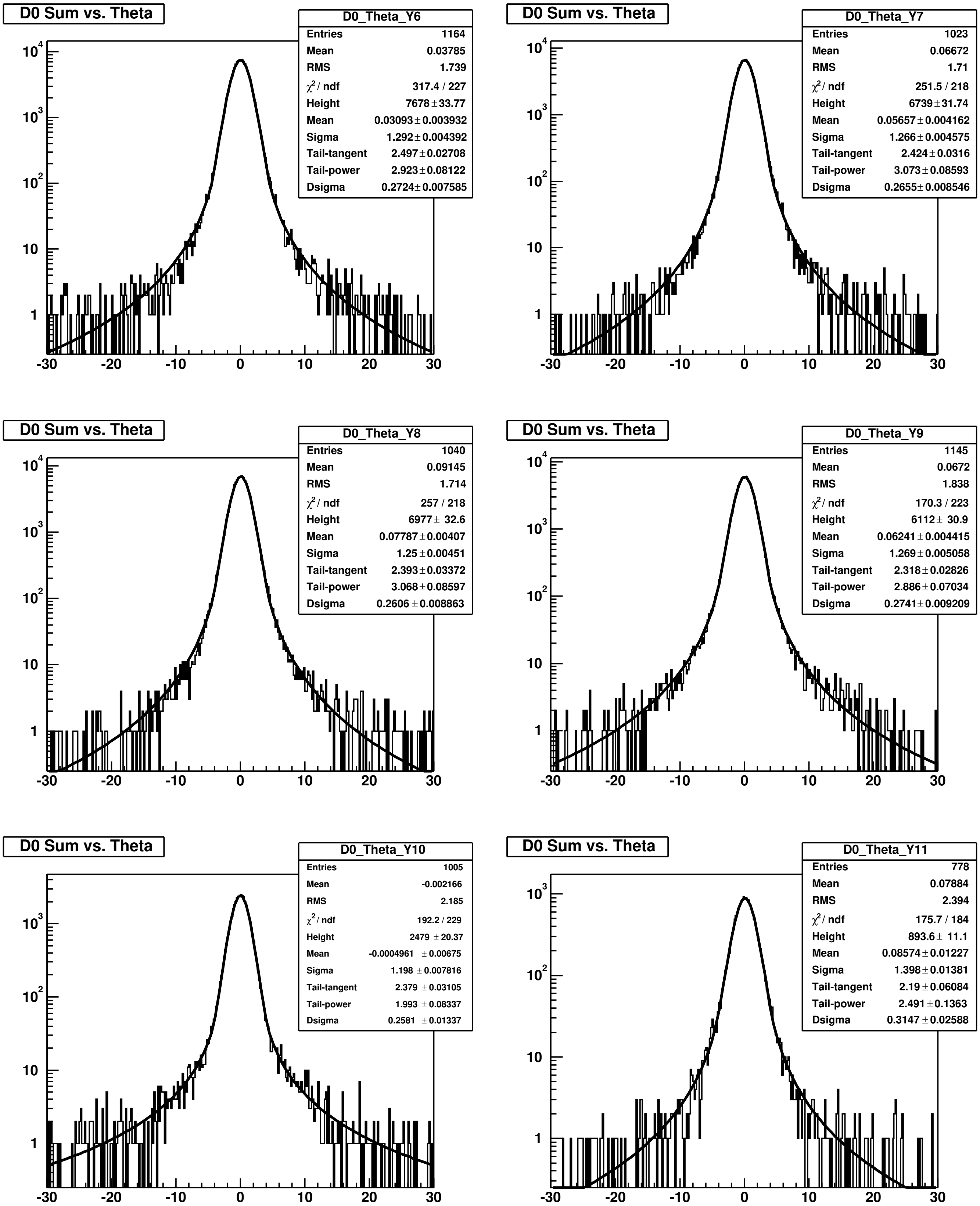

Figure 32: d_0 Sum divided by errors as a function of θ fit with equation 33

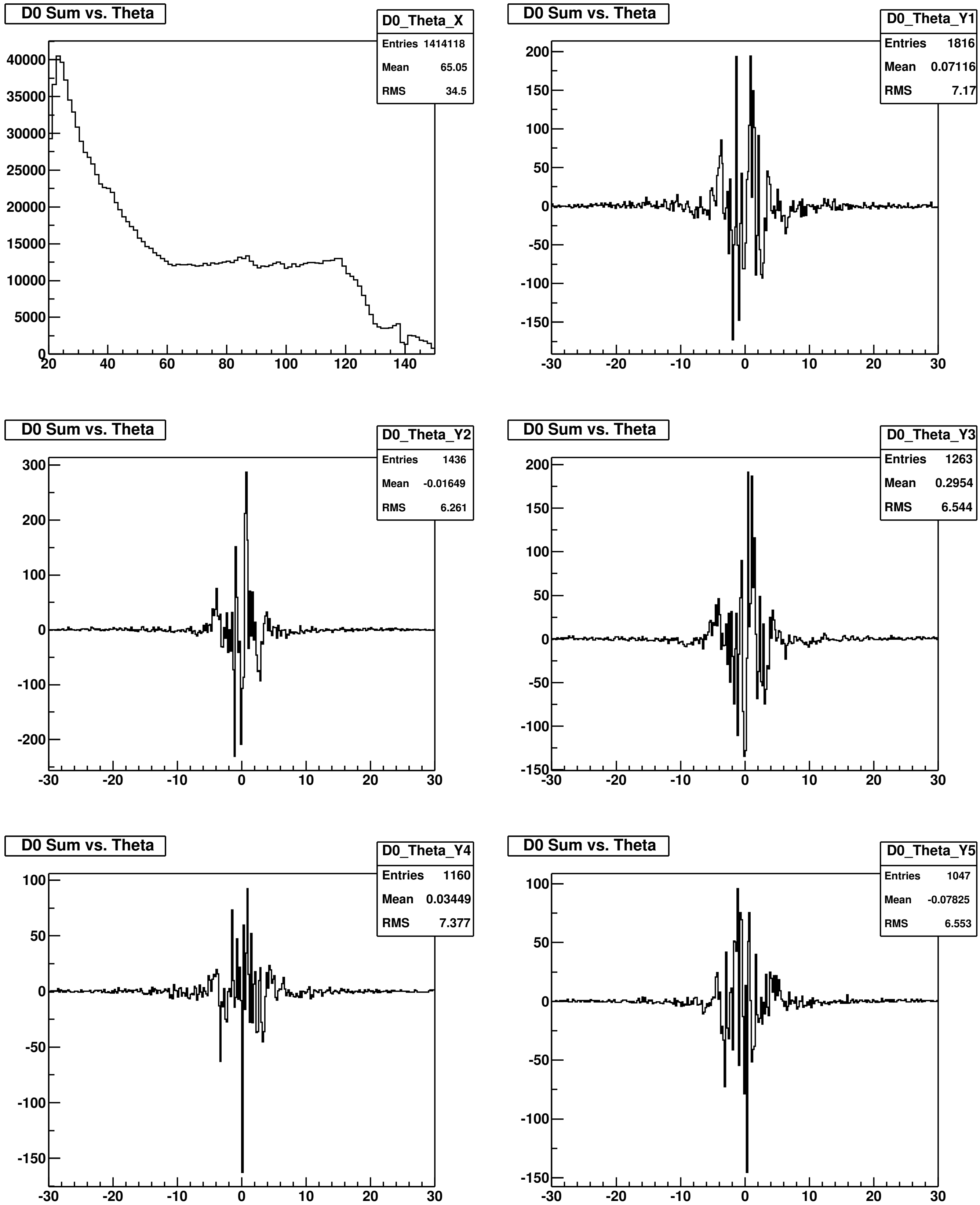

Figure 33: Residuals of d_0 Sum divided by errors as a function of θ fit with equation 33

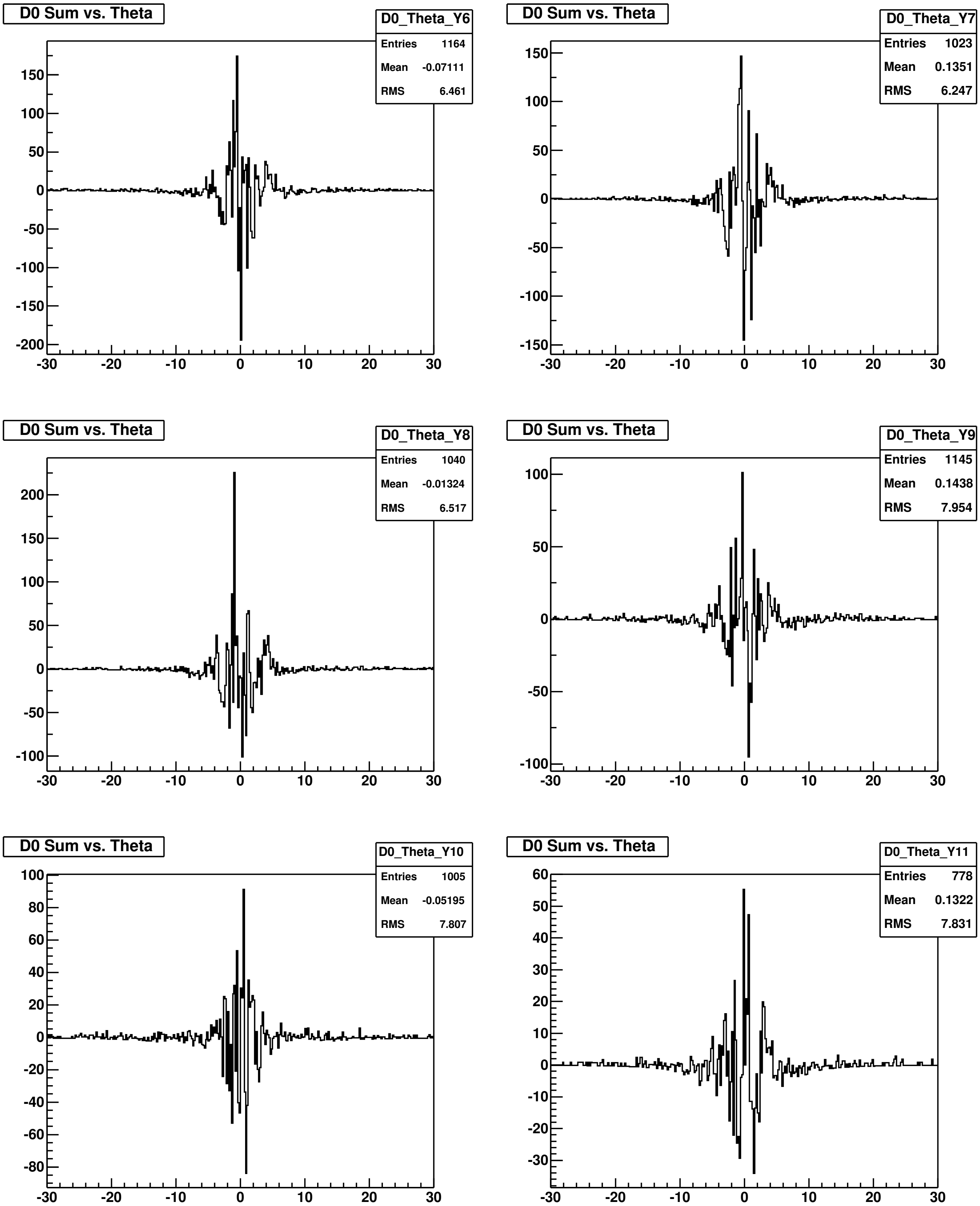

Figure 34: Residuals of d_0 Sum divided by errors as a function of θ fit with equation 33

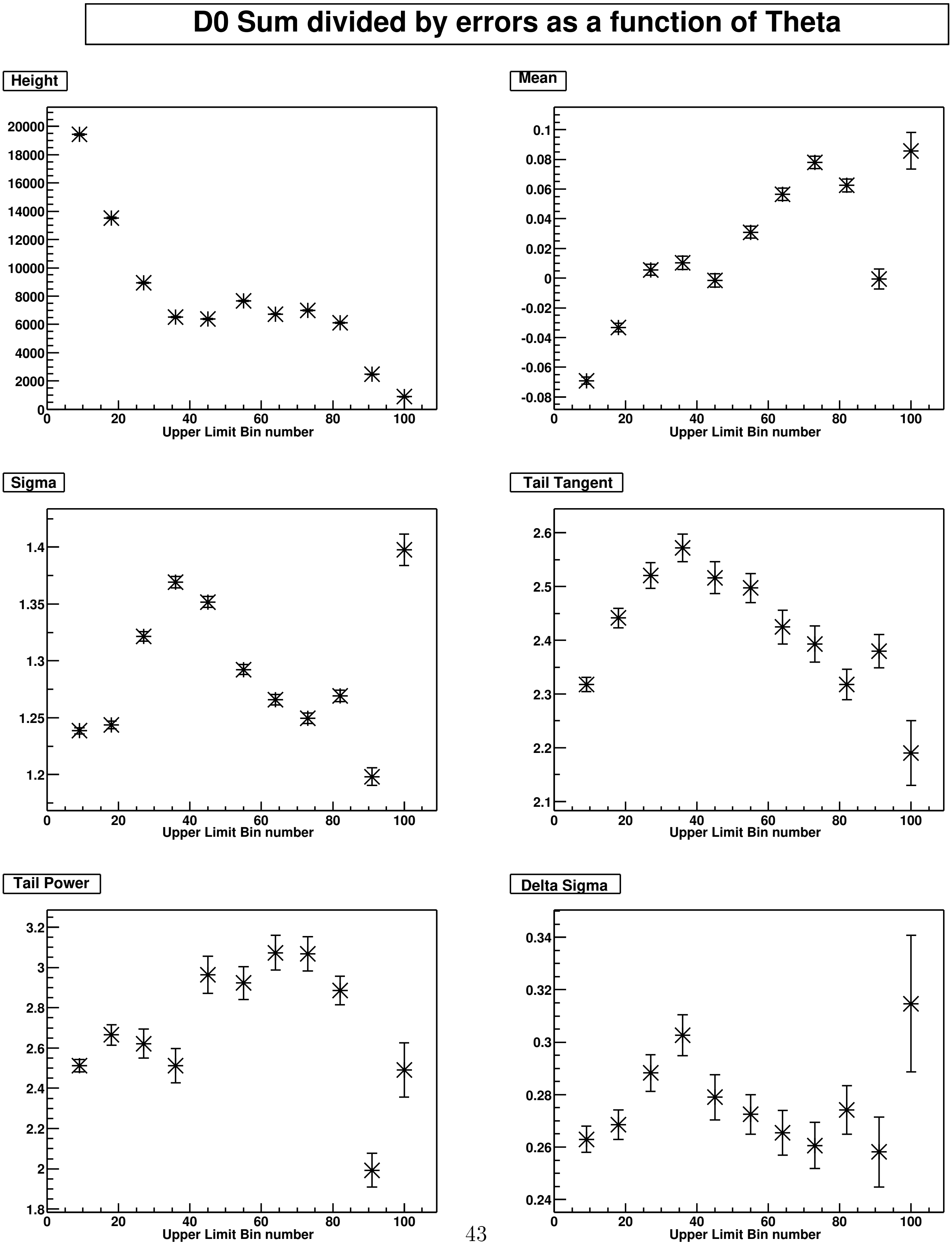

Figure 35: Parameters of equation 33 versus bin number for d_0 Sum divided by errors as a function of θ

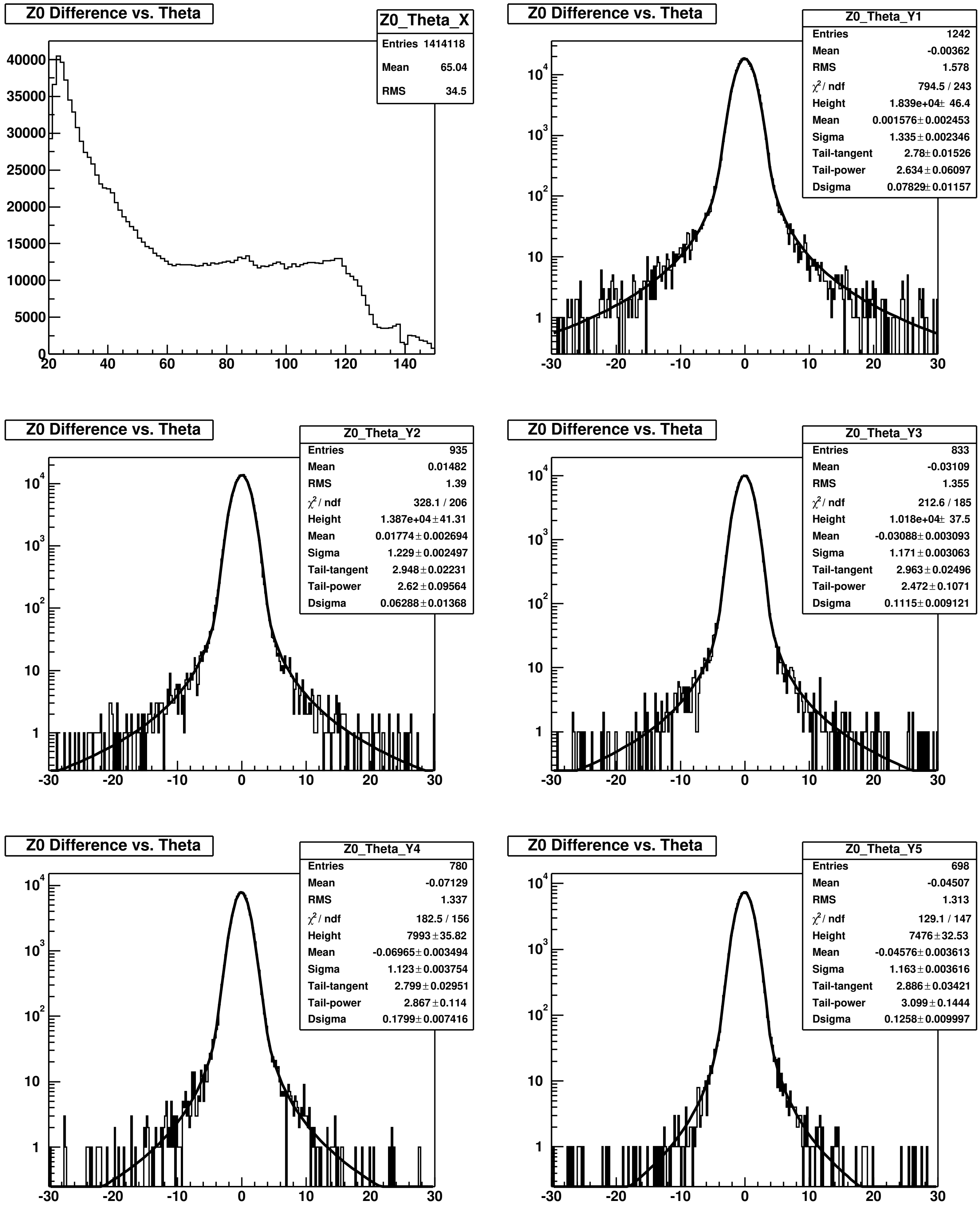

Figure 36: z_0 Difference divided by errors as a function of θ fit with equation 33

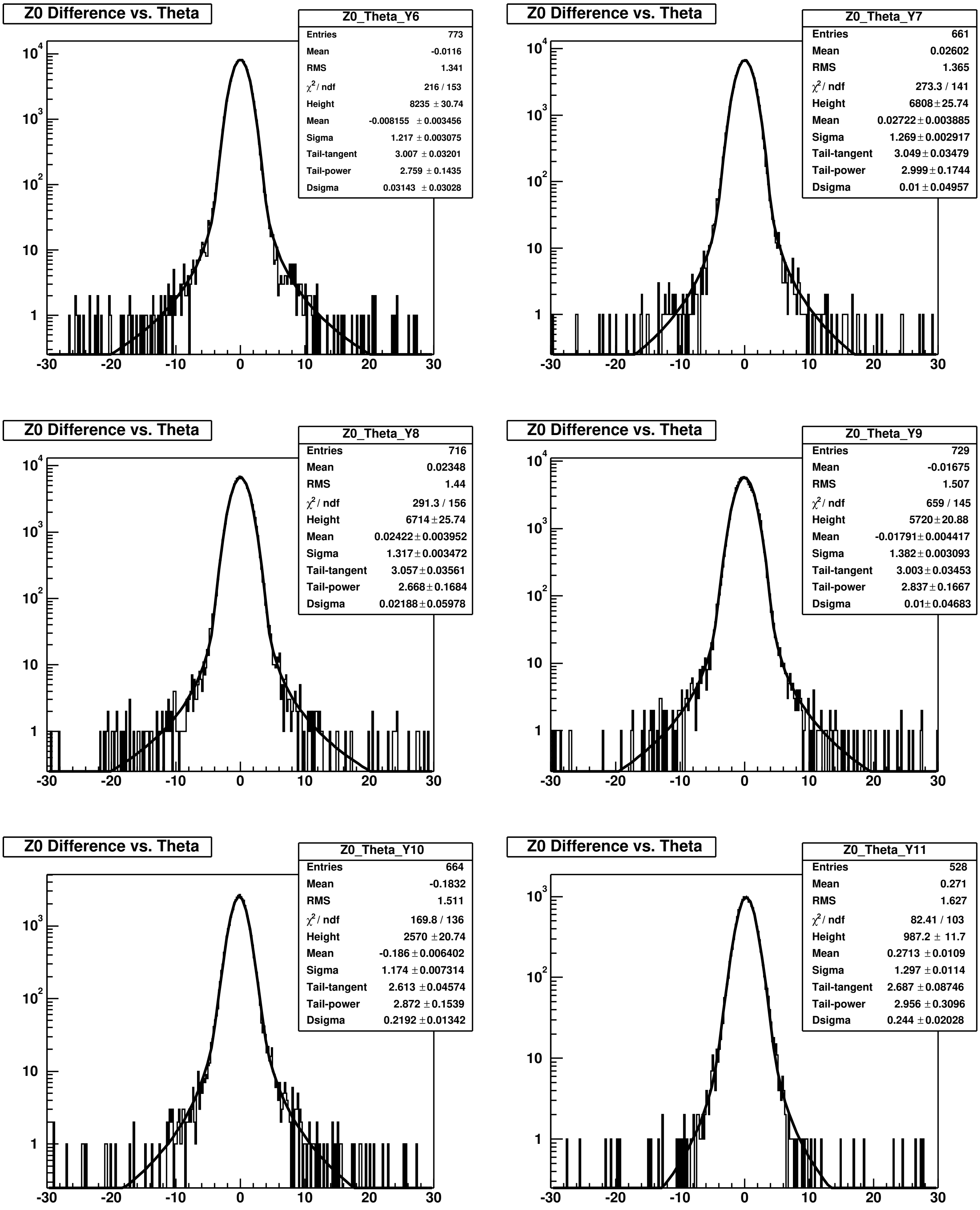

Figure 37: z_0 Difference divided by errors as a function of θ fit with equation 33

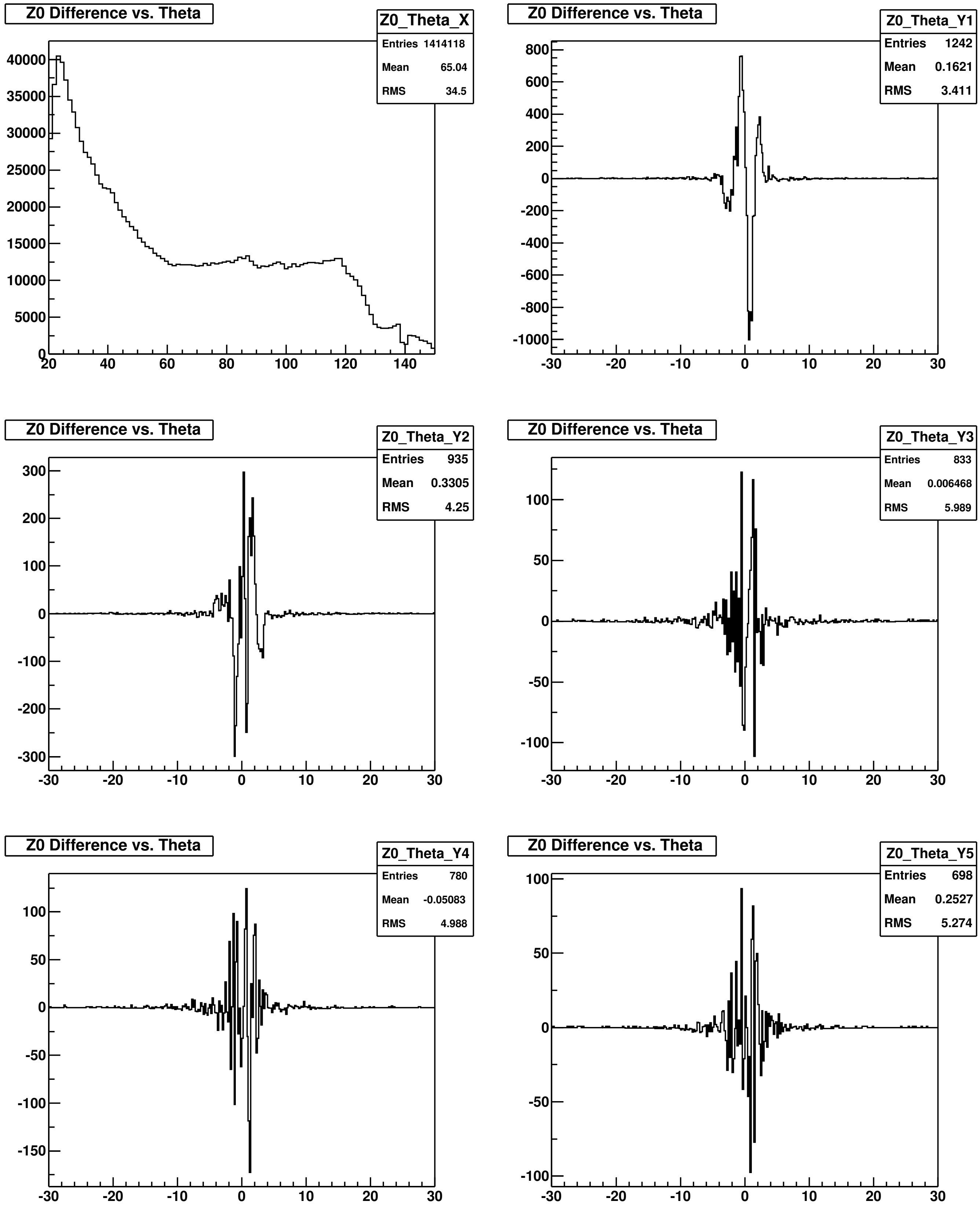

Figure 38: Residuals of z_0 Difference divided by errors as a function of θ fit with equation 33

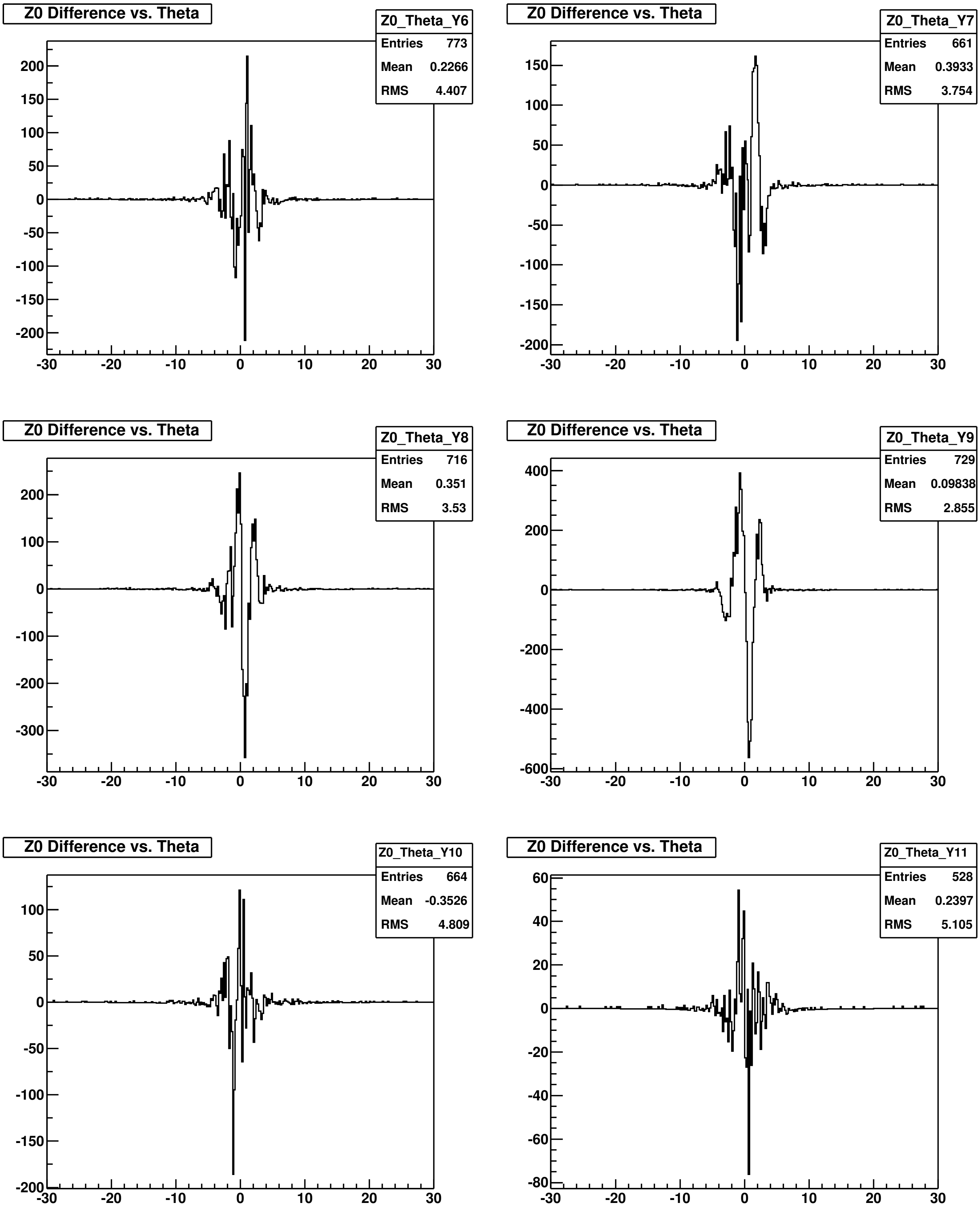

Figure 39: Residuals of z_0 Difference divided by errors as a function of θ fit with equation 33

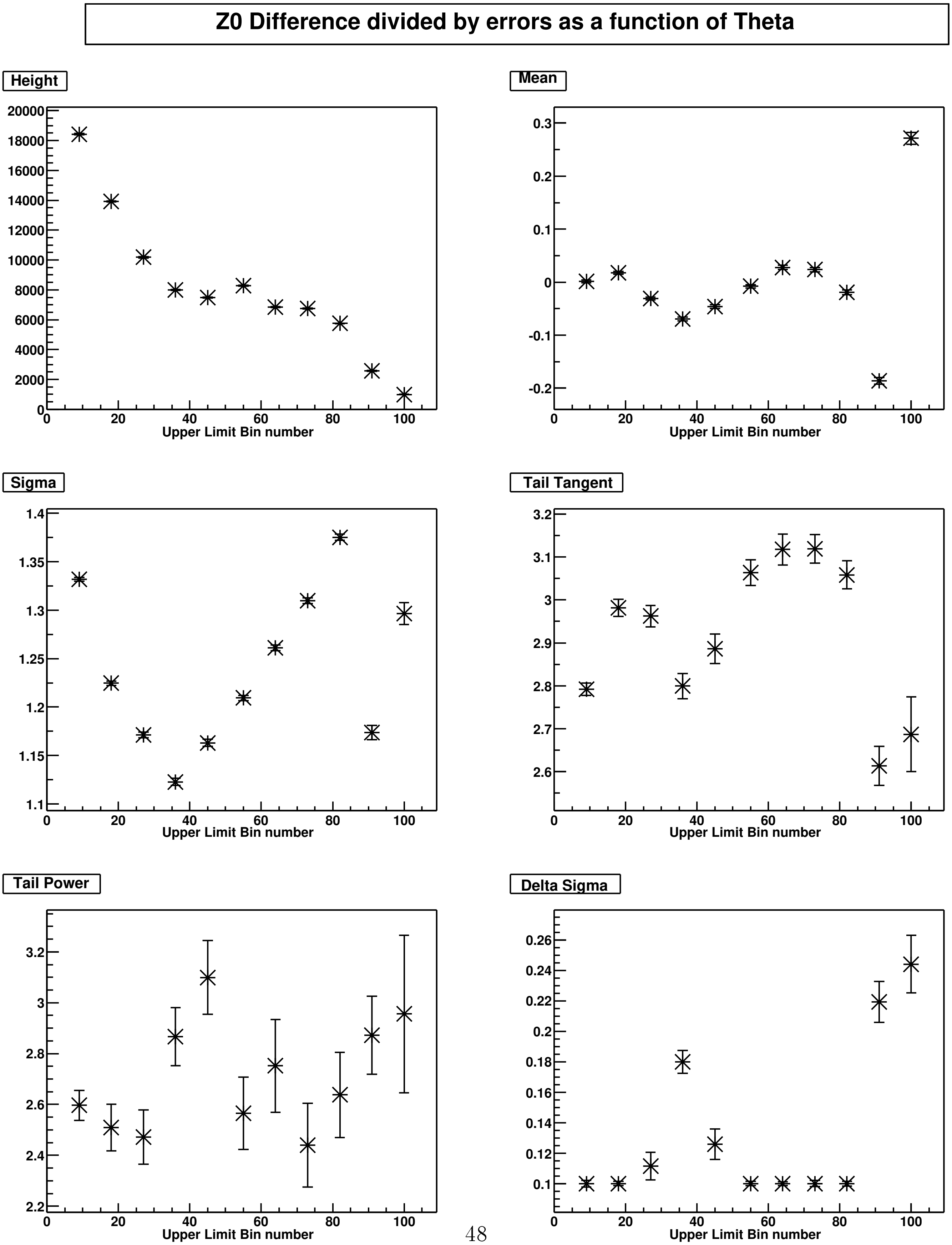

Figure 40: Parameters of equation 33 versus bin number for z_0 Difference divided by errors as a function of θ

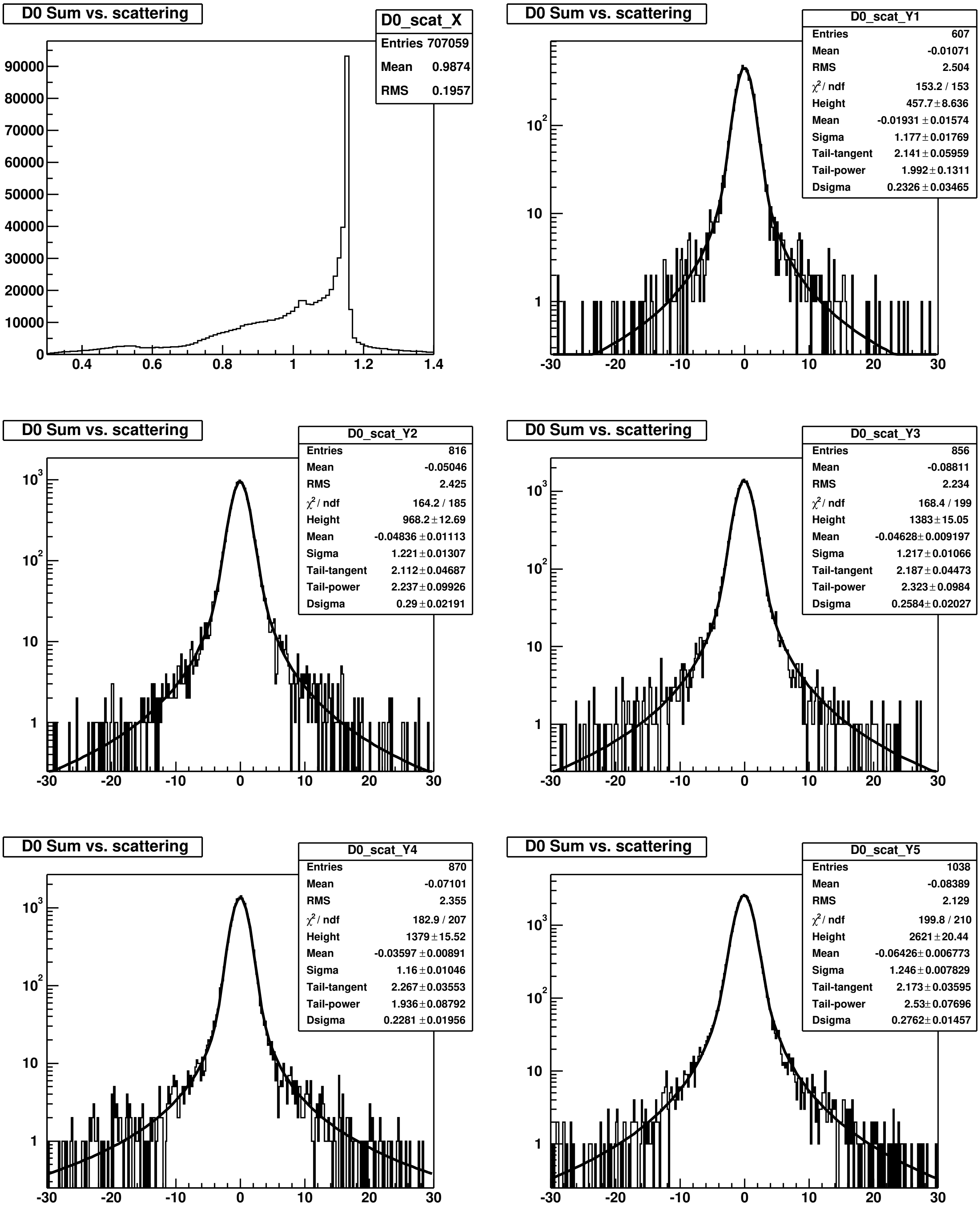

Figure 41: d_0 Sum divided by errors as a function of a scattering function (eq. 26) fit with equation 33

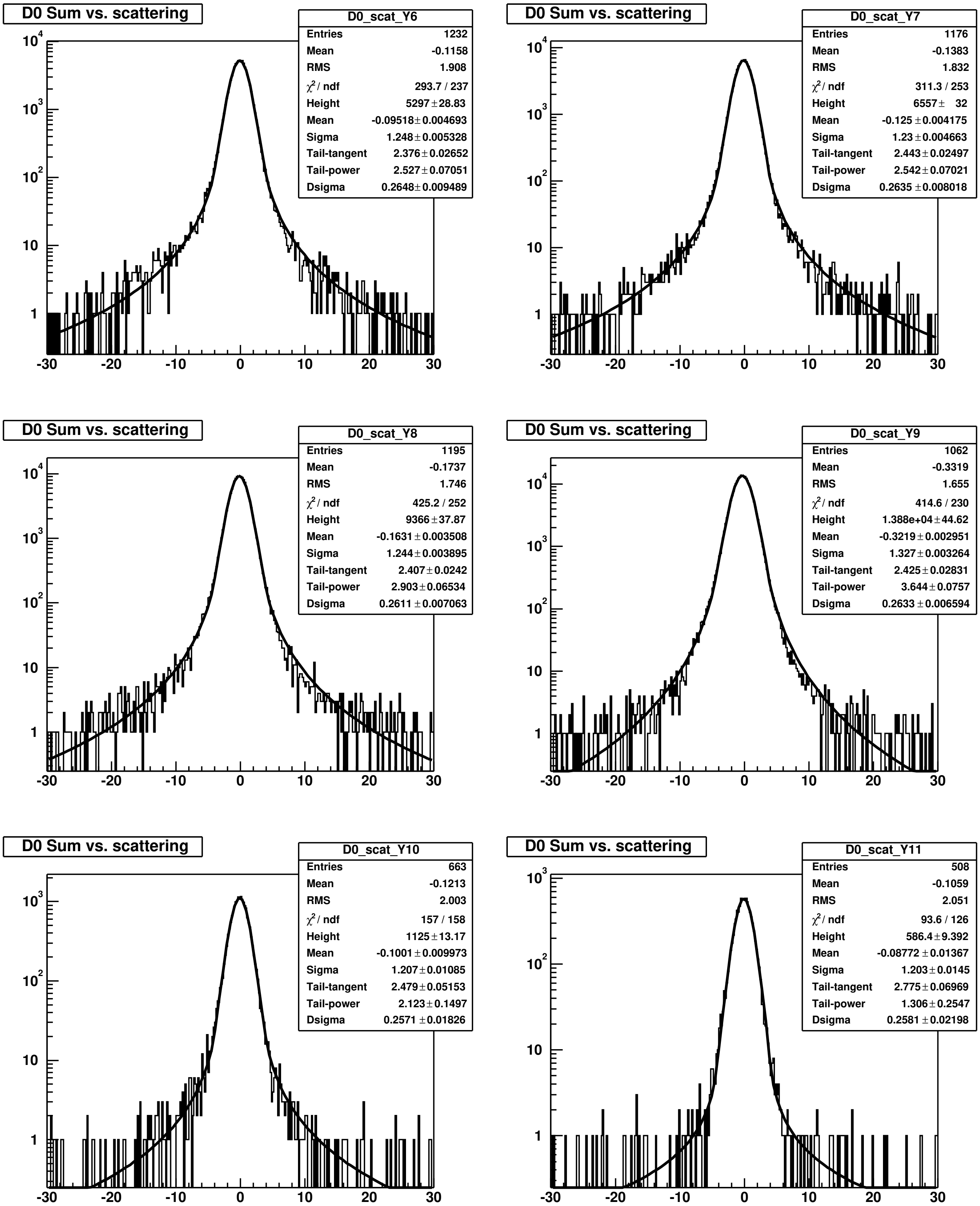

Figure 42: d_0 Sum divided by errors as a function of a scattering function (eq. 26) fit with equation 33

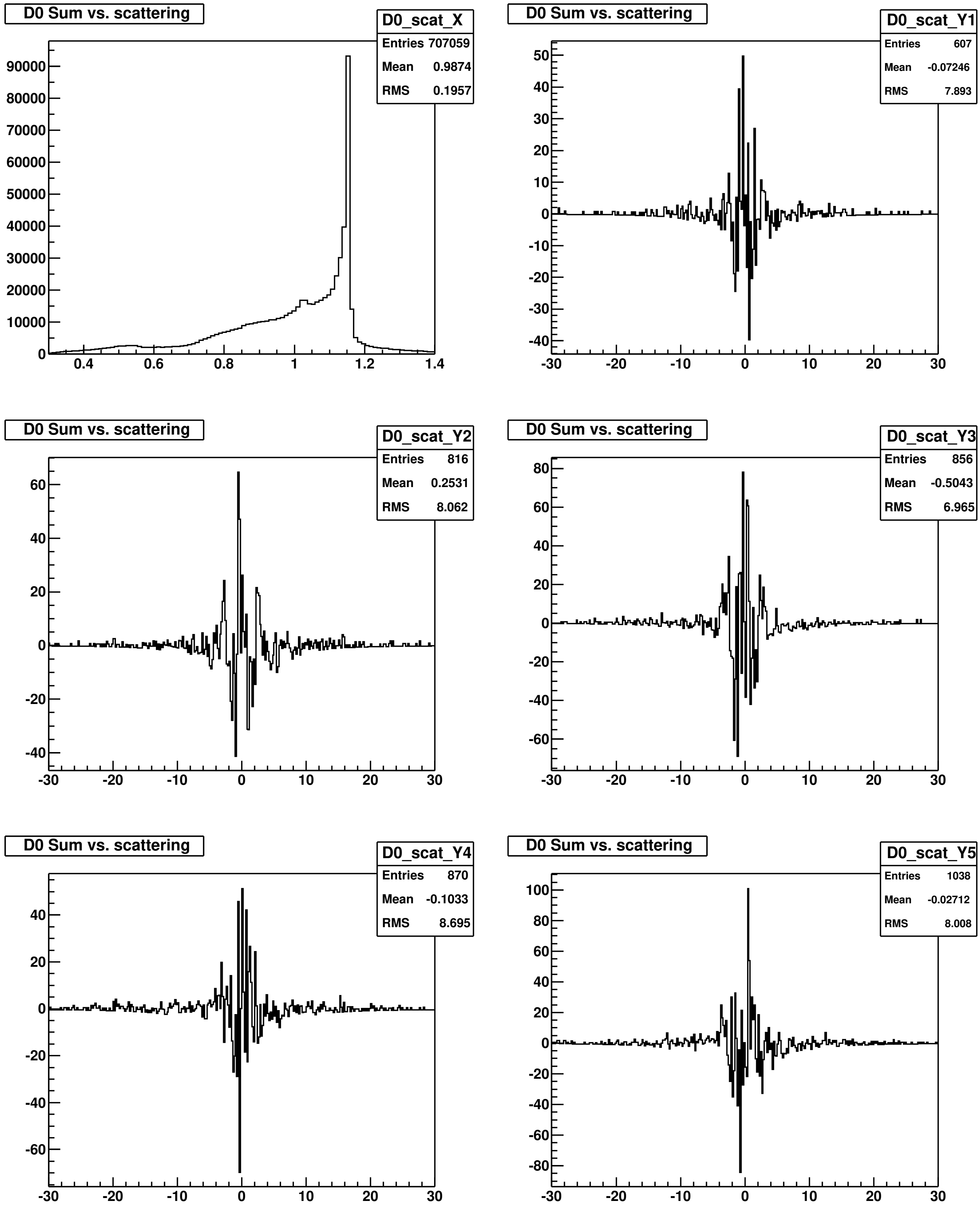

Figure 43: Residuals of d_0 Sum divided by errors as a function of a scattering function (eq. 26) fit with equation 33

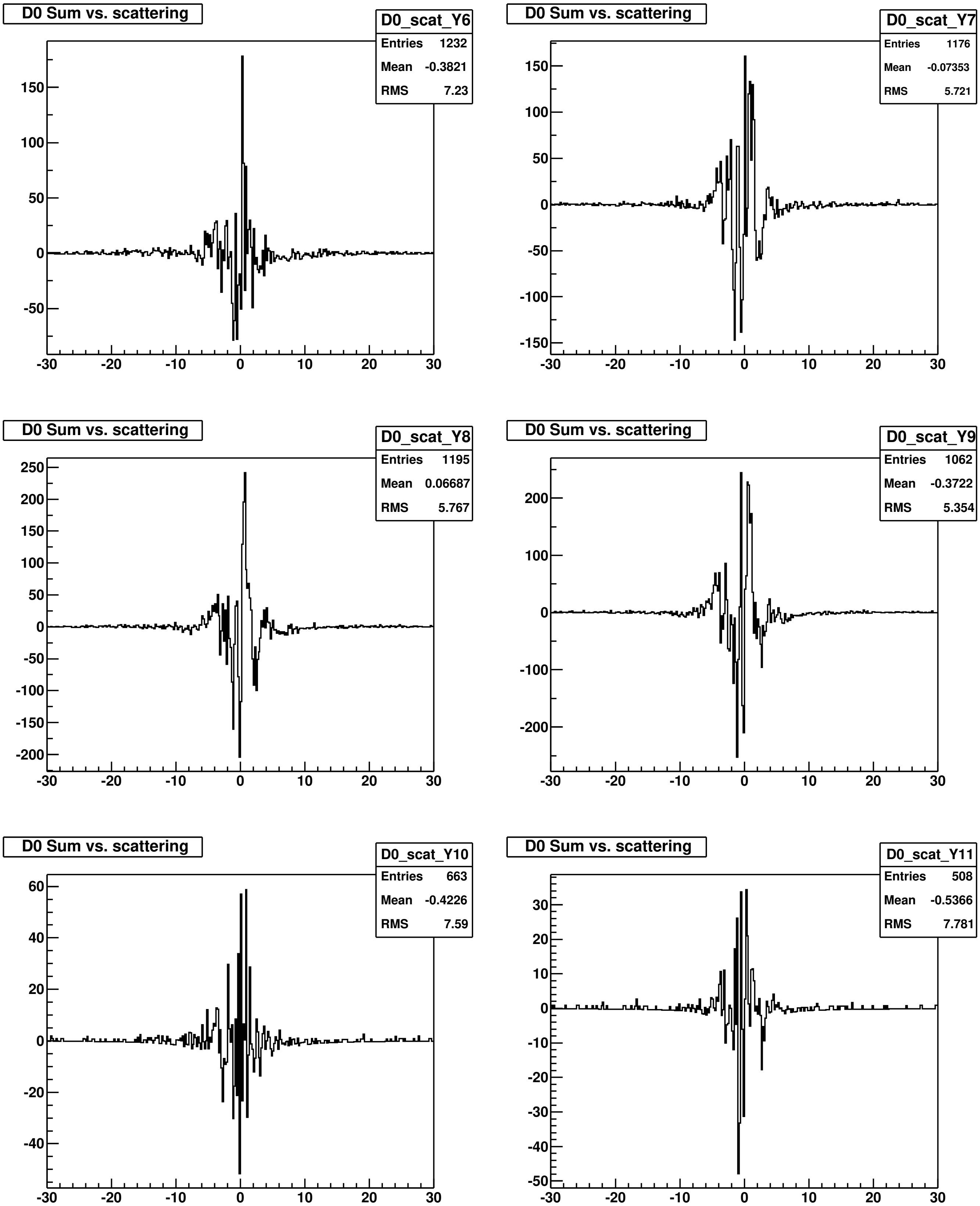

Figure 44: Residuals of d_0 Sum divided by errors as a function of a scattering function (eq. 26) fit with equation 33

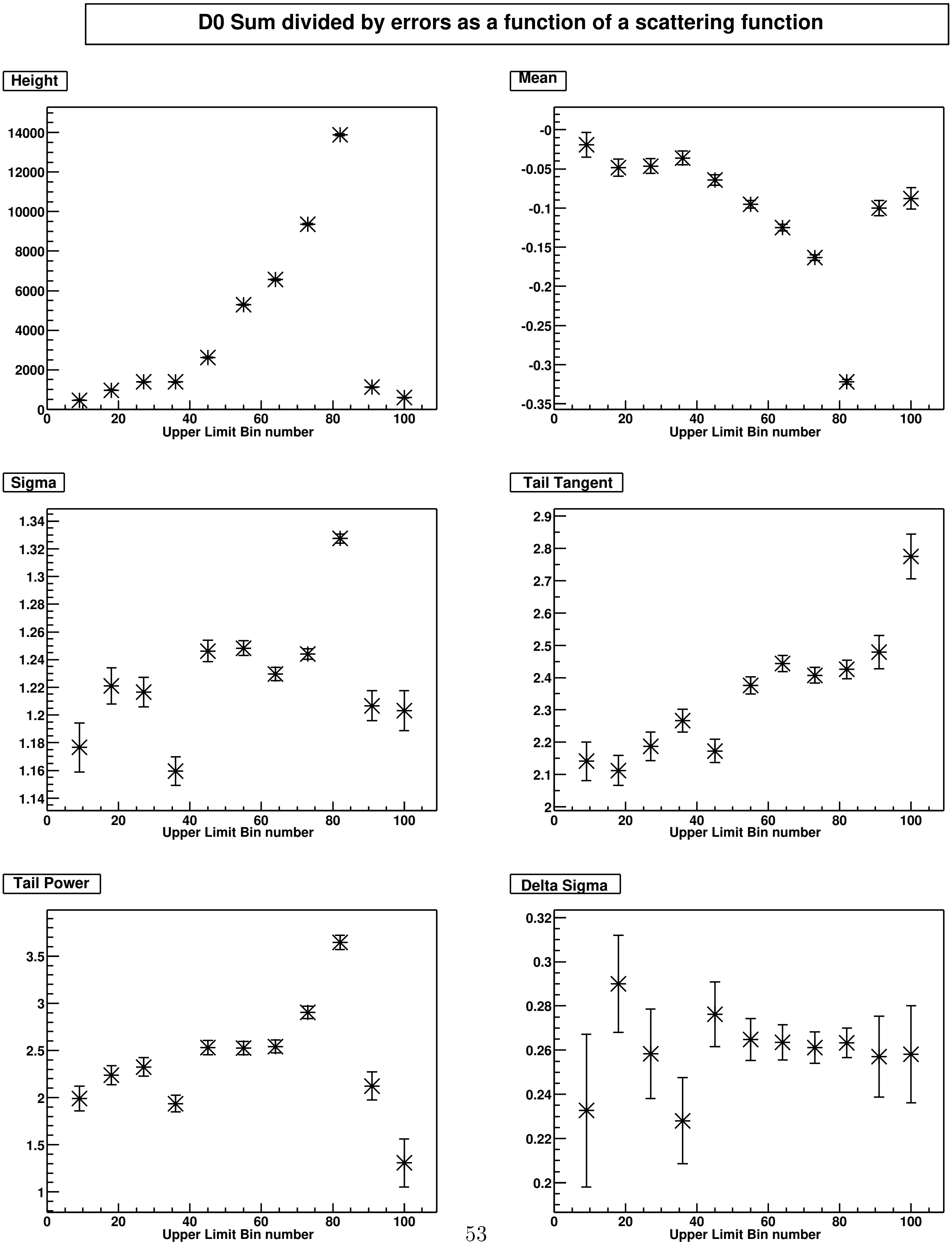

Figure 45: Parameters of equation 33 versus bin number for d_0 Sum divided by errors as a function of a scattering function (eq. 26)

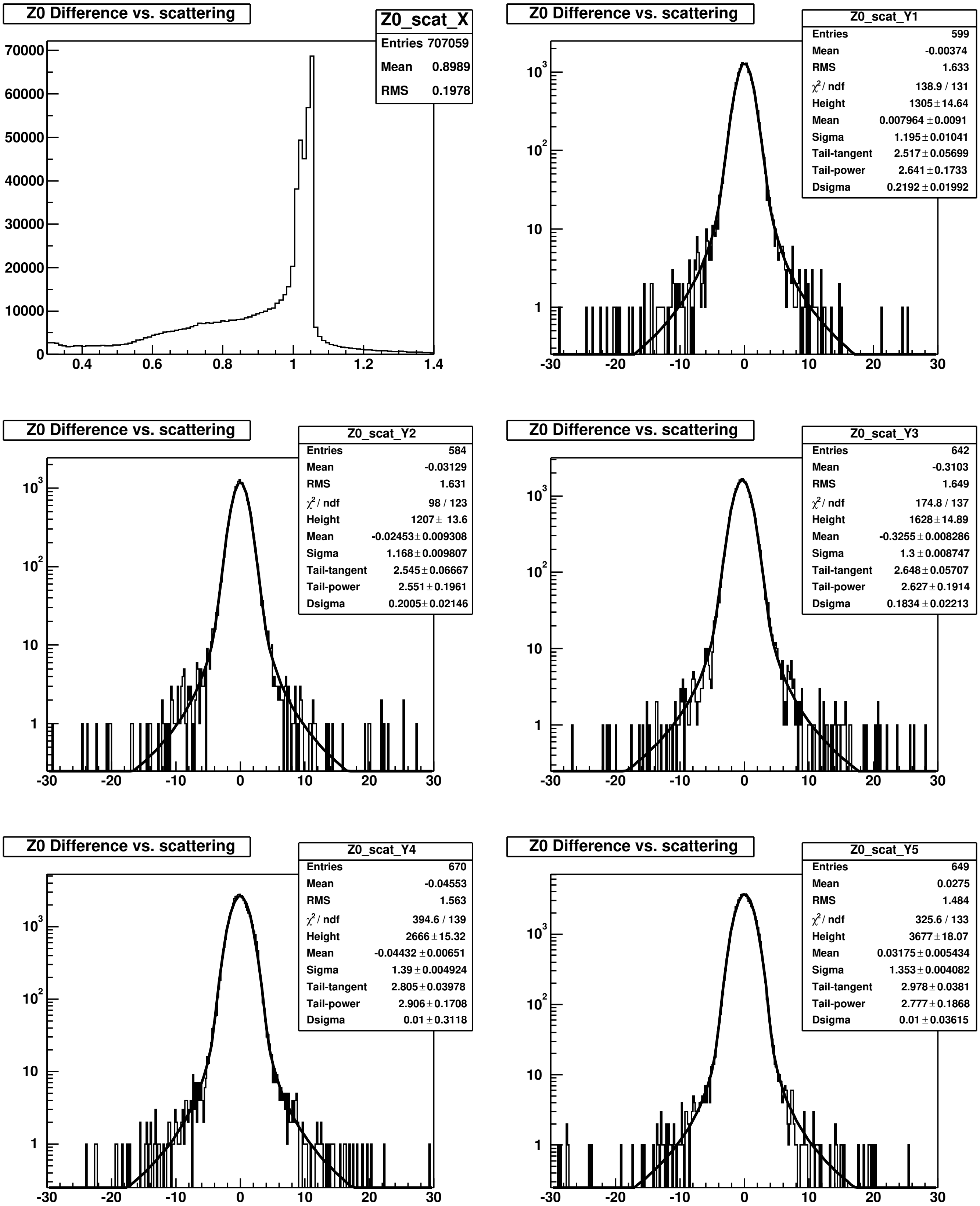

Figure 46: z_0 Difference divided by errors as a function of a scattering function (eq. 27) fit with equation 33

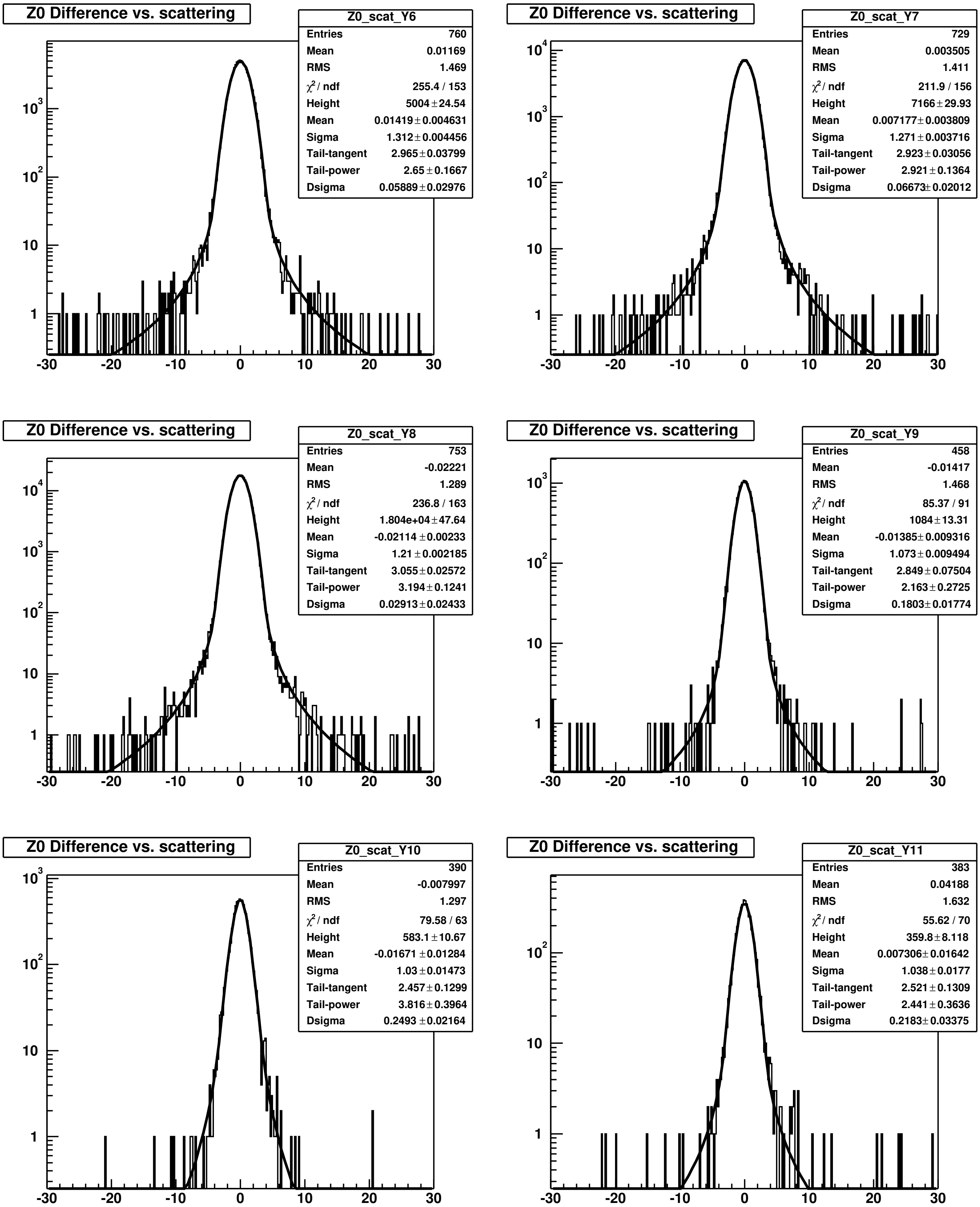

Figure 47: z_0 Difference divided by errors as a function of a scattering function (eq. 27) fit with equation 33

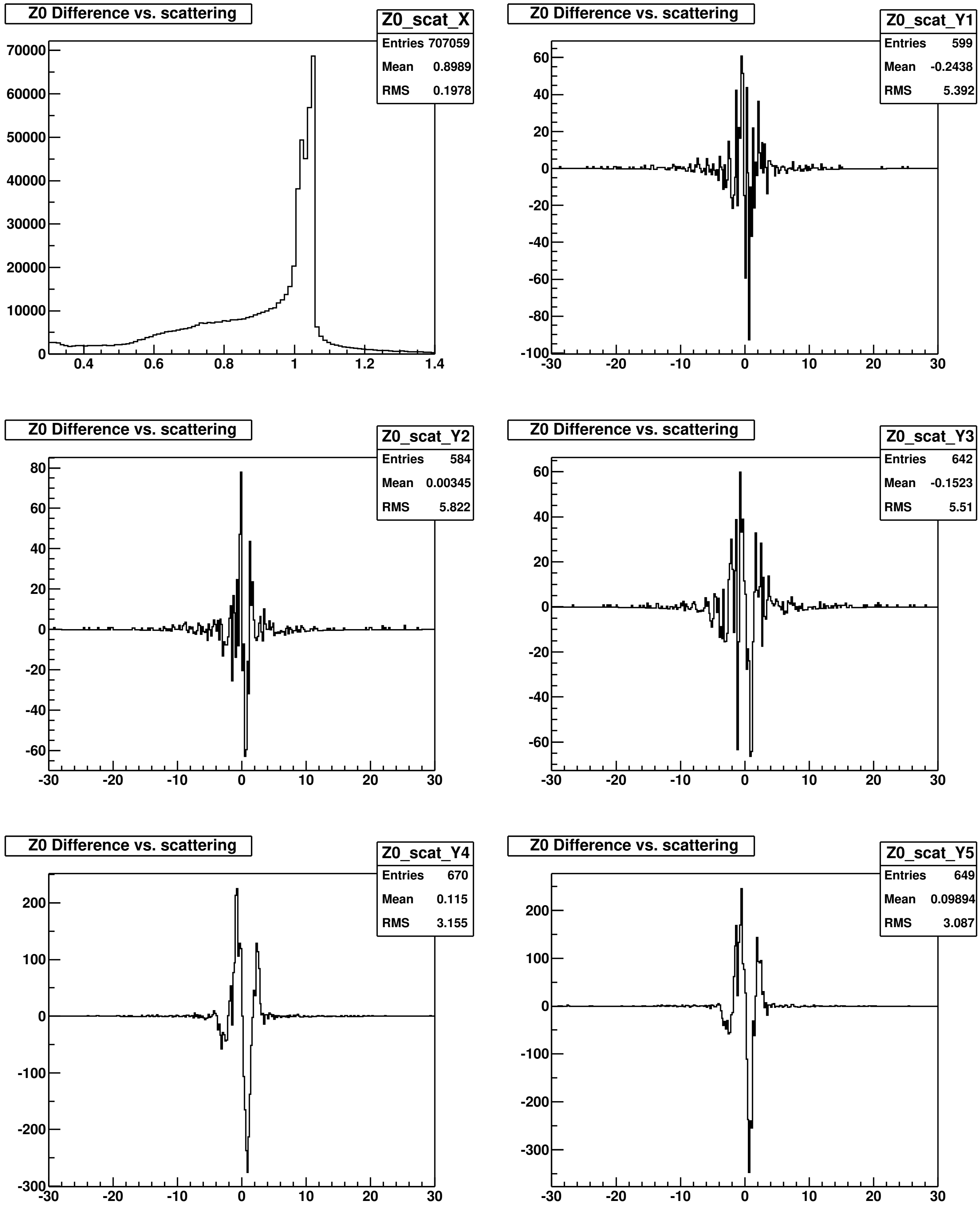

Figure 48: Residuals of z_0 Difference divided by errors as a function of a scattering function (eq. 27) fit with equation 33

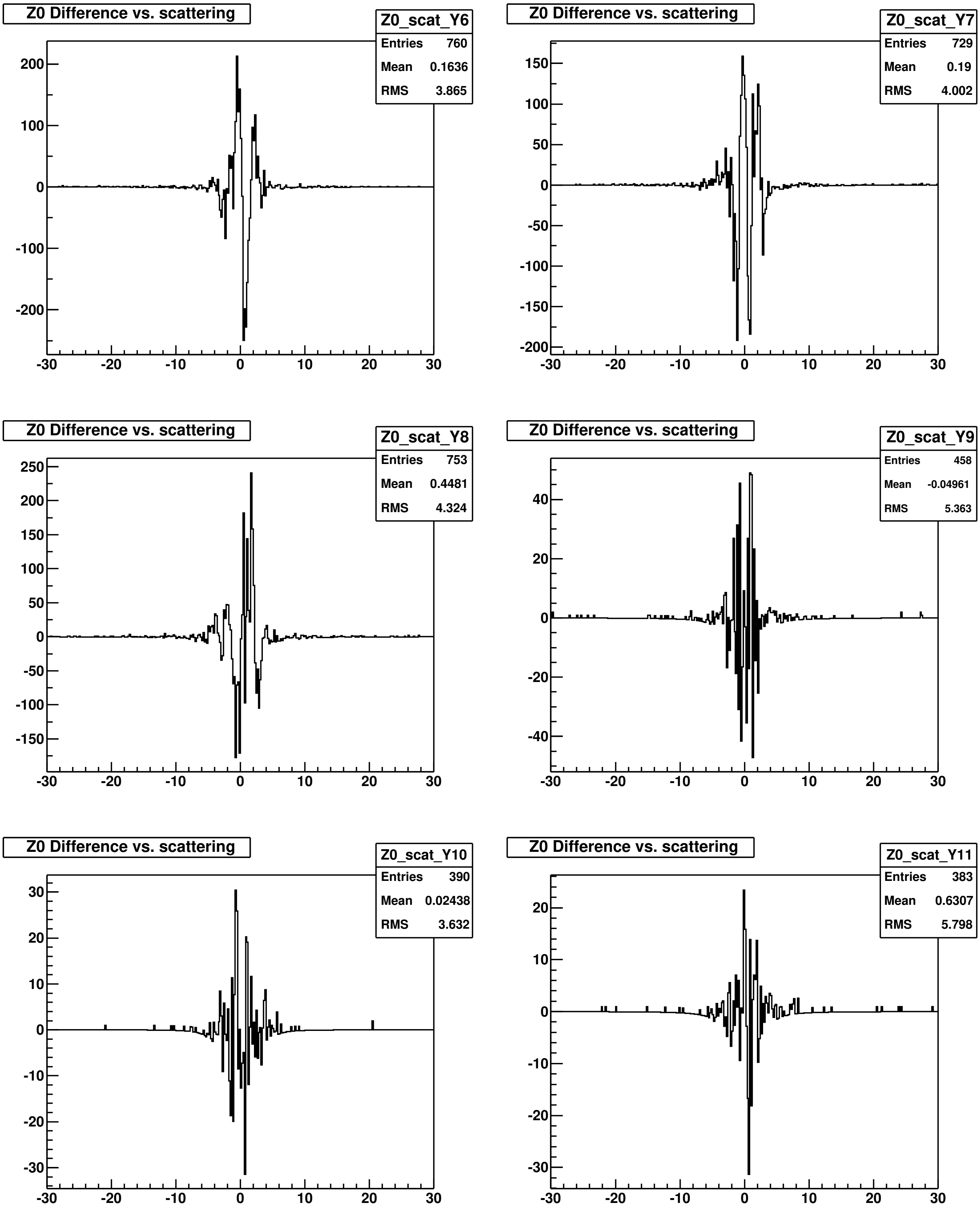

Figure 49: Residuals of z_0 Difference divided by errors as a function of a scattering function (eq. 27) fit with equation 33

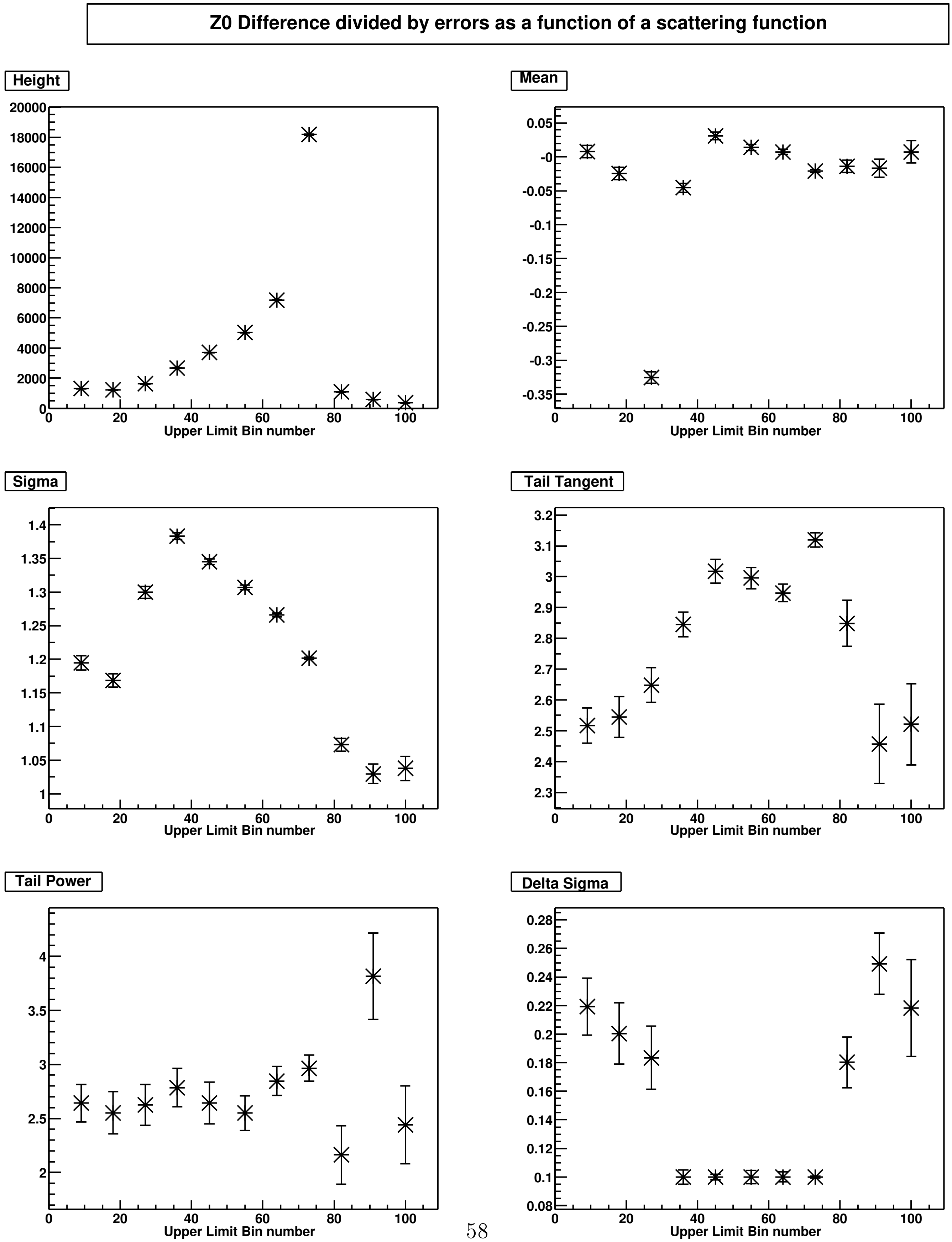

Figure 50: Parameters of equation 33 versus bin number for z_0 Difference divided by errors as a function of a scattering function (eq. 27)